Research Square

Preprints are preliminary reports that have not undergone peer review.
They should not be considered conclusive, used to inform clinical practice,
or referenced by the media as validated information.

Rethinking Urban Heat Risk through Objective–Subjective Heat Exposure Mismatch: An LCZ-Based Framework for Spatial Analysis and Associated Factors

yu Zhu
NWAFU: Northwest A&F University
Cailan Mo
NWAFU: Northwest A&F University
Zian Li
NWAFU: Northwest A&F University
Le Xuan
Dalian University of Technology
Bingshu Zhao
NWAFU: Northwest A&F University
Shengyu Meng
NWAFU: Northwest A&F University
Hongyi Luo
NWAFU: Northwest A&F University
Junran Wan
NWAFU: Northwest A&F University
Xuhui Wang
fywxuh@nwafu.edu.cn

NWAFU: Northwest A&F University
Tianhui Wang
NWAFU: Northwest A&F University

Research Article

Keywords: Local Climate Zone (LCZ), Subjective heat exposure, Urban heat risk, Social media data, BERT, Interpretable machine learning

Posted Date: November 5th, 2026

DOI: https://doi.org/10.21203/rs.3.rs-10866677/v1

License: This work is licensed under a Creative Commons Attribution 4.0 International License.
Read Full License

Additional Declarations: No competing interests reported.

Rethinking Urban Heat Risk through Objective–Subjective Heat Exposure Mismatch: An LCZ-Based Framework for Spatial Analysis and Associated Factors

Yu Zhu[a], Cailan Mo[a], Zian Li[a], Xuan Le[b], Bingshu Zhao[a], Shengyu Meng[a], Hongyi Luo[a], Junran Wan[a], Xuhui Wang[a,*], Tianhui Wang[a,*]

[a] School of Landscape Arts, Northwest A&F University, Yangling, Shaanxi,712100, China.

[b] School of Architecture and Fine Art, Dalian University of Technology, Dalian, 116024,China

[*]Corresponding author. School of Landscape Arts, Northwest A&F University, Yangling, Shaanxi,712100, China.

E-mail address: fywxuh@nwafu.edu.cn (Xuhui Wang)、wangth@nwafu.edu.cn （Tianhui Wang）; Tel: +8618591941811 (Xuhui Wang)

Abstract:

Increasing extreme heat events have highlighted the need to identify urban heat risks more accurately. However, existing assessments rarely examine whether such objective–subjective divergence is systematically associated with specific urban spatial contexts, limiting the identification of heat-risk blind spots that are not visible on conventional temperature maps.This study uses Xi'an's main urban area as a case, adopting the Local Climate Zone (LCZ) framework as a unified spatial analytical basis. By integrating Landsat-derived land surface temperature, population density, Weibo check-in texts, urban morphology, and public facility data, we construct population-weighted objective heat exposure (OHE) and BERT-based subjective heat exposure (SHE) indicators, the latter capturing observable public thermal perception from social media texts. The interpretable machine learning method CatBoost-SHAP is then applied to examine differences in the factors associated with OHE, SHE, and their deviation. Results show significant spatial mismatch between OHE and SHE across LCZ types: LCZ1, LCZ2, LCZ3, LCZ6, and LCZ7 are mainly characterized by High OHE–Low SHE, while LCZ4, LCZA, and LCZB show Low OHE–High SHE, indicating systematic deviation between objective and subjective heat exposure. OHE is primarily associated with physical factors such as building height, building density, and vegetation coverage, whereas SHE and its deviation from OHE show

stronger associations with socioeconomic conditions and the proximity of potential heat-adaptation resources. Impervious surface fraction and vegetation coverage also exhibit divergent response patterns between the OHE and SHE models, indicating that physical cooling effects do not necessarily translate directly into perceived heat relief. By treating objective–subjective heat mismatch as an explicit diagnostic dimension and using LCZs to organize the spatial contexts in which such divergence occurs, this study extends conventional temperature-hotspot assessment toward a multi-signal framework integrating physical exposure, observable thermal perception, and adaptation-related conditions. The proposed analytical logic provides a transferable approach for identifying locally specific heat-risk blind spots in other cities.

Key Words:Local Climate Zone (LCZ);Subjective heat exposure;Urban heat risk;Social media data;BERT;Interpretable machine learning

Highlights:

1.An LCZ-based framework revealed spatial mismatch between OHE and SHE.

2.Compact LCZs showed High OHE–Low SHE, while open and vegetated LCZs showed Low OHE–High SHE.

3.CatBoost-SHAP revealed divergent factor patterns of OHE, SHE and their mismatch.

4.Public service accessibility was associated with SHE beyond physical thermal conditions.

1. Introduction

With global warming and rapid urbanization, extreme heat has become a major threat to urban public health(Li, 2020). Studies have shown that high temperatures significantly increase the risks of heat stroke, cardiovascular diseases, and respiratory diseases, and lead to higher excess mortality(Dasgupta et al., 2024; Bogdanovich et al., 2023). To address increasingly severe heat risks, China's "National Climate Change Adaptation Strategy 2035" proposes strengthening urban thermal environment risk assessment and improving the precision of climate governance. Current urban heat governance mainly emphasizes green space development, blue-green infrastructure, ventilation corridors, and cooling facility allocation(Abd-Elmabod et al., 2024; Yin et al., 2025). However, heat risk assessments are still largely based on temperature-related indicators, while spatial differences in residents' thermal perception remain insufficiently considered. This limitation may lead to the underestimation of perceived heat risks and highlights the need to integrate objective exposure and subjective perception in urban heat risk assessment.

At present, urban heat exposure research mainly constructs objective heat exposure (OHE) indicators based on land surface temperature (LST). LST data retrieved from remote sensing sources such as Landsat and

ECOSTRESS (Zhang et al., 2025; Sun et al., 2024), due to their high spatial continuity and spatial resolution and their strong correlation with air temperature variations, are widely used to characterize the intensity of urban thermal environments (Huang et al., 2024; Zhang et al., 2018; Li et al., 2020). Under the same thermal environmental conditions, different population groups may vary significantly in individual characteristics, socioeconomic conditions, resource accessibility, and behavioral patterns, leading to substantial differences in their thermal perception and heat stress experience (Hass et al., 2022). Therefore, relying solely on objective temperature indicators is insufficient to fully capture the true spatial heterogeneity of urban heat risk.

To overcome this limitation, recent studies have increasingly explored subjective heat exposure (SHE) using questionnaire surveys and social media-based sentiment analysis. Questionnaire surveys can directly capture individual thermal perceptions and have been widely applied in thermal comfort studies(Ma et al., 2024; Zhang et al., 2021);but their limited sample size and high survey costs restrict large-scale and continuous assessments. In contrast, geotagged social media data combined with natural language processing provides an efficient approach for characterizing subjective thermal perception at the urban scale. In particular, sentiment analysis methods based on deep learning models such as BERT can identify heat-related emotional expressions

from massive text data and generate spatially continuous indicators of thermal perception. For example, Lyu et al. constructed a national-scale sentiment-based heat exposure map using Twitter data (Lyu et al., 2024), Wang et al. analyzed population sensitivity to heatwaves using social media data(Wang et al., 2021), and Liu et al. further compared spatial inequality differences between subjective and objective heat exposure(Qiqi Liu, Tian %J Sustainable Cities Hang, et al., 2025). These studies indicate that urban heat risk is reflected not only in differences in physical thermal conditions but also in variations in residents' perceived responses. However, existing studies have mainly focused on the separate characterization of OHE or SHE. The spatial mismatch between the two and the factors associated with its formation remain insufficiently explored, and the specific spatial contexts in which such mismatches occur are still not systematically understood.

Identifying the spatial mismatch between subjective and objective heat exposure requires comparing their response differences within a unified urban spatial context. The Local Climate Zone (LCZ) framework provides an effective spatial analytical unit for this purpose. Based on building height, building density, land cover, and anthropogenic activity characteristics, LCZ divides cities into spatial types with relatively consistent thermal environmental characteristics(Stewart & Oke, 2012). compared with traditional administrative units, LCZ can more directly

reflect the relationship between urban form and thermal environment and reduce the influence of spatial scale discrepancies on heat risk comparisons. LCZ types represent not only different thermal environments but also variations in urban functions, population activities, and access to public services(Guo et al., 2025), These differences may affect residents' activity patterns and cooling opportunities, resulting in divergent responses in thermal perception. Therefore, integrating OHE and SHE within the LCZ framework can help identify spatial mismatch patterns between physical heat exposure and perceived heat risk. Both OHE, SHE, and their mismatch are shaped by multiple environmental and social factors. Previous studies suggest that OHE is mainly associated with land cover and urban morphology(Wang et al., 2022), whereas SHE is additionally influenced by socioeconomic conditions, accessibility to services, cooling resources, and adaptive capacity(Qiqi Liu, Tian %J Sustainable Cities Hang, et al., 2025; Wang et al., 2022; Nan et al., 2025). Given the nonlinear interactions among these factors, traditional linear models may not fully capture their complex associations. This study therefore applies CatBoost with SHAP interpretation(Qiqi Liu, Tian Hang, et al., 2025) to examine the relationships between urban environmental factors and OHE, SHE, and their mismatch.

To address these gaps, this study uses Xi'an, a high-density city in western China, as a case study and integrates remotely sensed thermal

conditions, population distribution, social-media-based thermal perception, urban morphology, and public-service data within an LCZ-based analytical framework. Population-weighted land surface temperature is used to construct OHE, while Weibo texts and a BERT model are used to characterize SHE. Rather than examining OHE and SHE as two parallel indicators, the analysis focuses explicitly on where the two signals converge or diverge and how such divergence varies across different LCZ contexts. In doing so, the LCZ framework is extended beyond its conventional role in classifying physical thermal environments to provide a spatial context for organizing objective–subjective heat relationships. CatBoost-SHAP is further applied to compare the factors associated with OHE, SHE, and their deviation, allowing the analysis to distinguish the predominantly physical correlates of objective heat exposure from the broader environmental and adaptation-related conditions associated with subjective perception and mismatch. Through this integrated perspective, the study shifts the emphasis of urban heat assessment from identifying temperature hotspots alone toward diagnosing spatial blind spots where physical heat exposure and observable thermal perception do not coincide. More broadly, the proposed framework offers a transferable analytical logic for examining such locally specific mismatch patterns across different urban contexts.

2. Methods

The technical roadmap of this study is as follows：

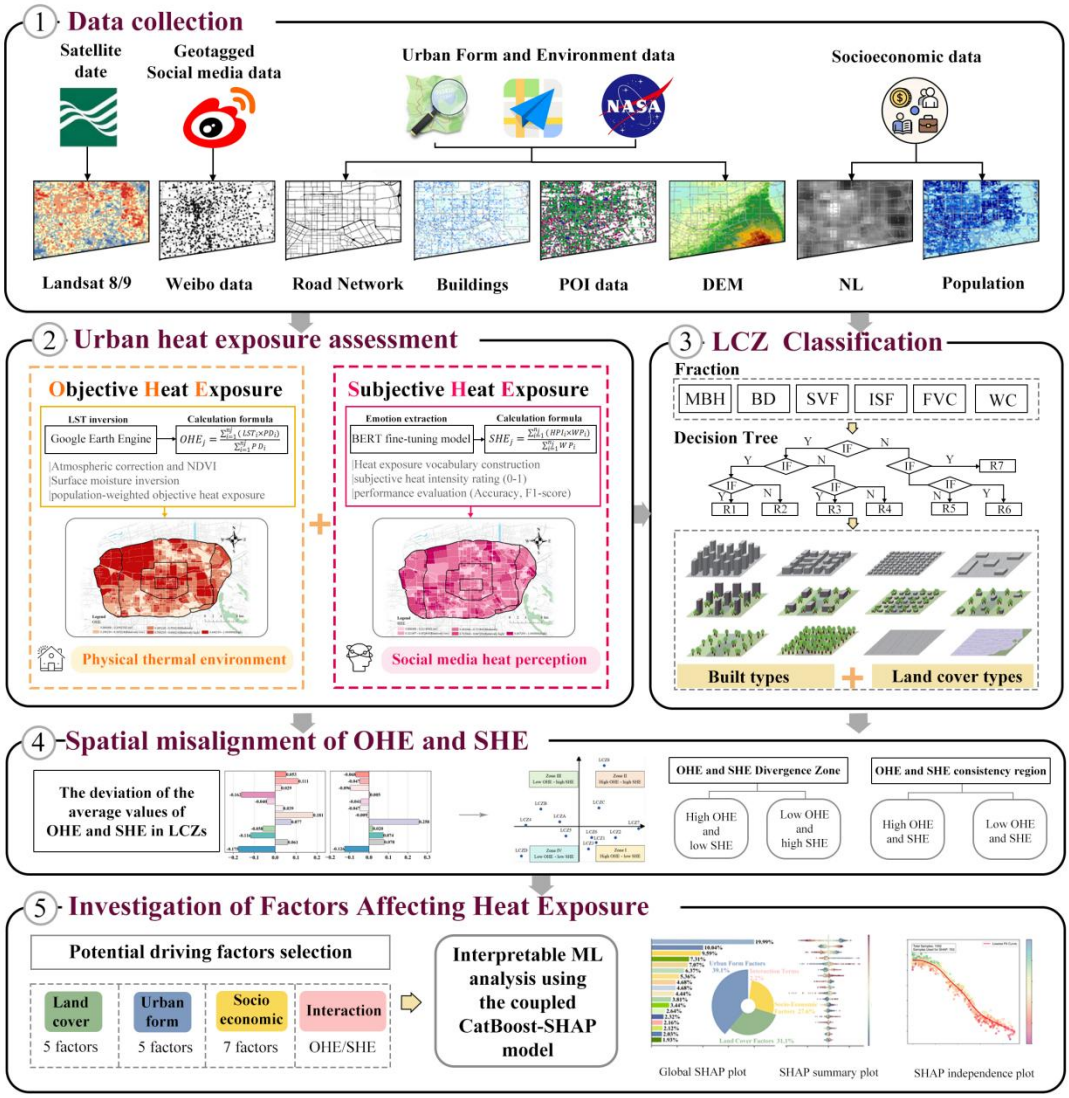


Figure 1 Workflow of this study

2.1 Study area and analytical units

This study selects the main urban area of Xi'an as the study area. Xi'an (107.4°–109.5°E, 33.5°–34.5°N) has a warm temperate semi-humid continental monsoon climate, characterized by hot summers with

historical extreme maximum temperatures exceeding 40°C; in recent years, it has frequently experienced persistent heat events, making it a typical high heat-risk city in China. As a representative rapidly urbanizing city in northwestern China, Xi'an has experienced expansion of built-up land and an increase in impervious surfaces in recent years, resulting in a complex urban spatial morphology that includes multiple LCZ types such as compact residential areas, open high-rise areas, commercial zones, industrial zones, and urban green spaces, providing a rich spatial context for comparing differences between objective heat exposure and subjective thermal perception across different spatial environments.

The study uses urban blocks as the basic analytical units, which are delineated into 1,082 blocks based on the OpenStreetMap road network. Block units can better reflect urban morphology and functional boundaries, facilitating the comparison of OHE, SHE, and their mismatch characteristics within a relatively homogeneous spatial context. This classification approach has received increasing attention in recent LCZ-based urban thermal environment studies(Yang et al., 2025).

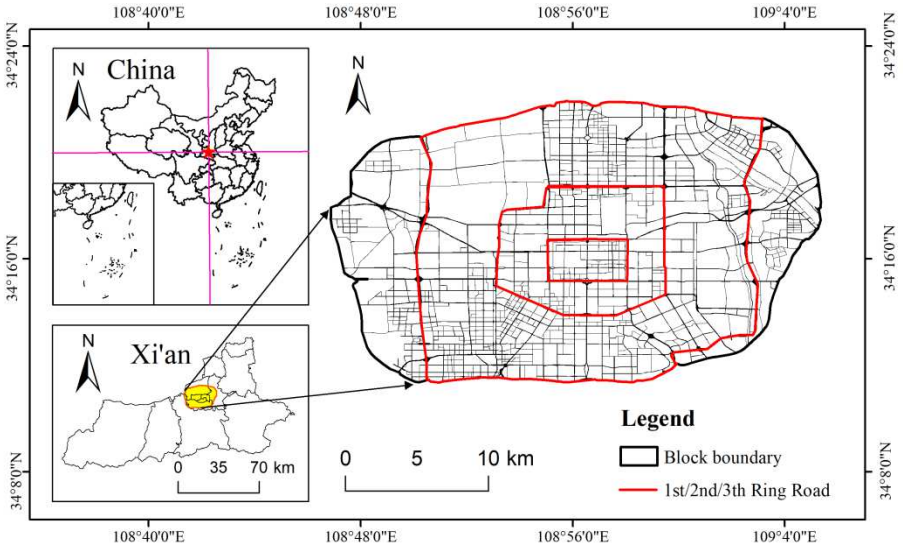


Figure 2 Overview of the study area

2.2 Data sources

This study integrates multi-source data, including remote sensing imagery, social media text, urban morphology, land cover, population density, nighttime lights, and public service facilities. Landsat 8/9 imagery is used to retrieve summer land surface temperature (LST) and extract land cover information; Weibo API data are used to identify public expressions of heat perception, and the data cleaning process removes low-activity nighttime data from 00:00–06:00 as well as invalid information such as advertisements, promotional content, and bot accounts; OpenStreetMap road data and Amap building data are used to delineate urban blocks and calculate urban morphology indicators; WorldPop population density and nighttime light data are used to represent exposed population and the intensity of socioeconomic

activities, respectively; Amap POI data are used to calculate accessibility to public services such as healthcare, commerce, culture, transportation, and emergency shelters. All spatial data are projected to a unified coordinate system, spatially clipped, and resampled to a consistent resolution before being aggregated to the block-level analytical units. These data are used to reveal the spatial heterogeneity of heat exposure and its underlying sources of spatial variation; detailed descriptions of the datasets are provided in Table 1.

Table 1 Data sources and descriptions

Data category	Data source	Time period	Spatial resolution	Main purpose
Remote sensing data	https://earthexplorer.usgs.gov/	June–August 2025	30 m	Acquisition of land surface temperature and land cover data
Social media data	http://weibo.com	June–August 2025	Georeferenced point data	Extraction of heat-related affective expressions and construction of subjective heat exposure
Road network data	https://www.openstreetmap.org	2025	Vector	Urban block delineation
Building data	https://lbs.amap.com/	2025	Vector	Morphological indicators such as building height, density, and proximity
POI	https://lbs.amap.com/	2025	Vector	Facility accessibility (medical, shelter, commercial, etc.)
Nighttime light data	https://dataverse.harvard.edu/	2024	500 m	Proxy indicator of socioeconomic capacity
Population	https://www.worldpop	2023	100 m	Exposed population size

Data category	Data source	Time period	Spatial resolution	Main purpose
density data	.org			
DEM	http://srtm.csi.cgiar.org/srtmdata/	2025	30 m	Derivation of topographic factor

2.3 Construction of objective and subjective heat exposure

To compare spatial response differences between physical thermal environment exposure and residents' thermal perception, this study constructs OHE and SHE indicators, respectively.

OHE represents population-weighted land surface heat exposure under the urban physical thermal environment. This study integrates LST and population density to construct a population-weighted OHE indicator(Feng et al., 2024), representing the spatial distribution of potential heat exposure. Landsat 8/9 images with less than 10% cloud cover during June–August 2025 were obtained from Google Earth Engine. LST was retrieved using the single-channel algorithm, and multi-temporal summer images were composited to characterize the overall thermal conditions of the study area. LST and population density data were then resampled to 150 m resolution, and population density was used as the weight to calculate population-weighted OHE values for each grid cell. This approach incorporates the influence of spatial population distribution in thermal environment representation and is more suitable

for studying spatial heterogeneity of heat exposure at the urban scale. The calculation formula is shown in Equation (1):

$$OHE_j = \frac{\sum_{i=1}^{nj}(LST_i \times PD_i)}{\sum_{i=1}^{nj} P\,D_i} \quad (1)$$

Where OHE_j is the OHE value of grid cell j;nj is the total number of raster cells within the grid; LST_i is the land surface temperature of raster cell i; and PD_i is the population density of measurement point i.

SHE is used to represent observable public thermal perception responses derived from social media text. First, a heat-related keyword lexicon is constructed based on direct thermal perception terms, high-temperature state descriptions, and colloquial expressions, and is further expanded using WordNet and ConceptNet (Appendix S1). On this basis, the BERT-Chinese-Base model is used for heat-related text identification and sentiment intensity analysis. The BERT model has strong language representation capability (Subakti et al., 2022), making it suitable for identifying implicit thermal perception expressions in social media text, and it has been widely applied in heat-related text studies(Qiqi Liu, Tian %J Sustainable Cities Hang, et al., 2025; Dou et al., 2024). Text identification is conducted in two stages: the first stage identifies heat-related texts, and the second stage quantifies thermal perception sentiment intensity. To improve annotation reliability, 500

samples are randomly selected from heat-related texts and annotated by two independent annotators (sentiment intensity is assigned on a five-level 0–1 scale, where higher values indicate stronger negative thermal perception); the Cohen's Kappa coefficient is 0.82, model accuracy is 92.0%, and the macro-average F1-score is 0.88. The model outputs are transformed into continuous 0–1 scores using the Sigmoid function, where higher values indicate stronger thermal perception. The methodological workflow is shown in Figure 3.

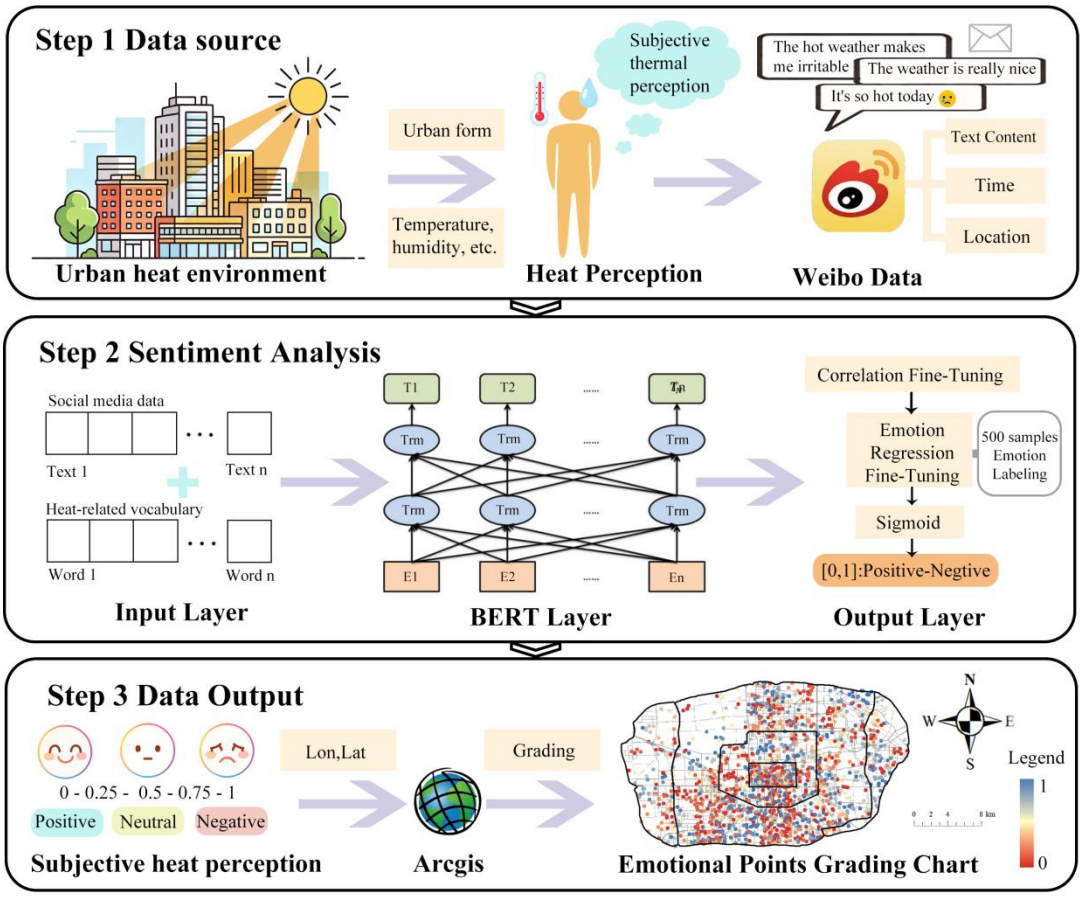


Figure 3 Workflow diagram of subjective heat exposure scoring

Considering differences in Weibo post volumes across different urban blocks, this study constructs SHE by jointly considering the proportion of heat-related texts and sentiment intensity(He et al., 2025), and the calculation formula is as follows (2):

$$SHE_j = \frac{\sum_{i=1}^{n_j}(HPI_i \times WP_i)}{\sum_{i=1}^{n_j} WP_i} \quad (2)$$

Where SHE_j is the SHE value of grid cell j; nj is the number of heat-related Weibo posts; HPI_i is the thermal perception intensity score of Weibo post i; and WP_i represents the proportion of heat-related Weibo posts to total posts, used to weight the contribution of each post.

To ensure comparability between OHE and SHE, both are normalized and rescaled to a 0–1 range (Equation 3), establishing a unified comparison scale for subjective and objective heat exposure and providing a consistent basis for subsequent spatial comparison and differentiation analysis.

$$UHE_n = \frac{X_i - \min X_i}{\max X_i - \min X_i} \quad (3)$$

2.4 Analysis of spatial mismatch characteristics of OHE and SHE based on LCZ

2.4.1 Construction of the LCZ spatial framework

This study adopts the LCZ as a unified spatial classification framework. LCZ classification is based on indicators such as building height, building density, sky view factor, impervious surface ratio, vegetation cover, and water proportion, and is implemented using a decision tree method(Chen et al., 2020), in combination with the LCZ framework proposed by Stewart and Oke (Figure 4)(Stewart & Oke, 2012) and existing classification results for Xi'an(Yuan et al., 2022; Yunwei Zhang et al., 2020) for localized classification; detailed parameter values are provided in Table 2. Considering the actual distribution of LCZ types, categories with limited representation were integrated. To validate the reliability of the classification results, 200 sample points were randomly selected and visually interpreted using high-resolution remote sensing imagery, street view imagery, and building morphology data, and classification accuracy was evaluated using overall accuracy (OA) and the Kappa coefficient.



Figure 4 Standard LCZ types(Stewart & Oke, 2012). 1–10 represent built types, and A–G represent land cover types.

Table 2 LCZ types and classification indicators

LCZs	MBH(m)	BD(%)	SVF	ISF(%)	FVC(%)	WC(%)
Compact high-rise(LCZ1)	>30	25-60	0.2-0.6	>40	<40	<10
Compact mid-rise(LCZ2)	15-30	25-60	0.2-0.6	>30	<40	<10
Compact low-rise(LCZ3)	3-15	25-60	0.2-0.6	>30	<40	<10
Open high-rise(LCZ4)	>30	10-25	0.4-0.8	20-70	20-50	<10
Open mid-rise(LCZ5)	15-25	10-25	0.4-0.8	30-70	20-50	<10
Open low-rise(LCZ6)	3-15	10-25	0.4-0.8	20-70	20-50	<10
Sparsely built(LCZ7)	3-15	10-25	>0.7	20-50	20-70	<10
Large low-rise(LCZ8)	3-15	>50	>0.7	50-90	10--30	<10
Sparsely vegetated area(LCZA)	-	<10	>0.8	<10	20-90	<10
Dense vegetated area(LCZB)	-	<10	>0.8	<10	>90	<10
Bare rock or paved(LCZC)	-	<10	>0.9	>80	10-30	<10
Water(LCZD)	-	<10	>0.9	<10	<10	>40

2.4.2 Identification of LCZ-based mismatch types between subjective and objective heat exposure

Within a unified LCZ spatial framework, this study further identifies the spatial matching and mismatch types of OHE and SHE. First, the

deviation values of OHE and SHE for each analytical unit relative to the study area average are calculated, and based on the direction of these deviations, four categories are defined: High OHE–High SHE, High OHE–Low SHE, Low OHE–High SHE, and Low OHE–Low SHE (Table 3). When the deviation directions of OHE and SHE are consistent, it indicates a relative match between subjective and objective heat exposure; when the directions are opposite, it indicates a mismatch between them. This classification is used to identify the matching relationships and spatial mismatch characteristics of OHE and SHE across different LCZ types.

Table 3 Classification of mismatch types between subjective and objective heat exposure

Type	Condition
High OHE and low SHE	△OHE>0 and △SHE<0
Low OHE and high SHE	△OHE<0 and △SHE>0
High OHE and SHE	△OHE>0 and △SHE>0
Low OHE and SHE	△OHE<0 and △SHE<0

2.5 Analysis of differences in the associated factors of subjective–objective heat exposure mismatch

2.5.1 Selection of dependent and independent variables

To further elucidate the influencing mechanisms of subjective and objective heat exposure and their spatial mismatch, this study constructs three dependent variables for associated factors analysis. First, OHE and

SHE are separately used as dependent variables to compare differences in their driving factors between objective and subjective heat exposure. Second, to directly characterize the relative deviation between the two and explore the associated factors of mismatch, a mismatch index (D) is constructed:

$$D = SHE - OHE \quad (4)$$

Where D is used solely to represent the relative deviation between subjective and objective heat exposure, serving spatial pattern comparison and driving factor identification, and does not represent an absolute temperature or perception difference. Furthermore, this study focuses on modeling the D index in two types of mismatch areas—High OHE–Low SHE and Low OHE–High SHE—to identify the factors potentially associated with mismatches between OHE and SHE responses.

For the dependent variable analysis, this study selects potential driving factors from three dimensions: land cover, urban morphology, and social environment. Land cover factors reflect surface thermal environmental characteristics, urban morphology factors represent building structure and spatial organization characteristics, and socioeconomic factors describe residents' resource accessibility and potential social vulnerability. The definitions and calculation methods of

353 all variables are provided in Table 4. All variables are aggregated to the
354 block scale and standardized prior to modeling.

355 Subsequently, the differences in the effects of each driving factor on
356 OHE, SHE, and the mismatch index D are compared to identify the
357 associated factor patterns of subjective–objective heat exposure and their
358 spatial mismatch.

359 Table 4 Types of potential factors influencing heat exposure

Types	Factors	Abbreviation	Processing method	Notes
Land use(Lan et al., 2022; Huang et al., 2025; Mondal et al., 2025)	Accessibility to blue space	ABS	Euclidean distance	Distance to cooling spaces affects local temperature
	Accessibility to green space	AGS	Euclidean distance	
	Impervious surface fraction	ISF	$ISF=S/S_{site}$	Absorbs and stores heat, intensifying the urban heat island effect
	Vegetation coverage fraction	FVC	$FVC=\frac{NDVI-NDVI_m}{NDVI_{max}-NDVI}$	Vegetation reduces land surface temperature through evapotranspiration and shading
	Elevation	DEM	—	Elevation and slope affect ventilation and air temperature
Urban morphology(Zhou et al., 2022)	Building height	MBH	$MBH=\frac{\sum_{i=1}^{n} BS_i{}'' BH_i}{\sum_{i=1}^{n} BS_i}$	Urban morphology jointly determines local ventilation conditions, shading effects, and heat accumulation
	Building density	BD	$BD=\frac{\sum_{i=1}^{n} BS_i}{S_{site}}$	
	Sky View Factor	SVF	$SVF=\frac{\sum_{i=1}^{n} SVF_i}{n}$	
	Building proximity	PROX	$PROX=\frac{\sum \bar{d}_i}{n}$	
	Average Height Standard Deviation	AHSD	$AHSD=\sqrt{\frac{\sum_{i=1}^{n}(BH_i-M}{n}}$	
Socioeconomic (Qunyue Liu et al., 2025; Zeng et	Population density	POP	—	Represents the size of population exposed to high temperatures

Types	Factors	Abbreviation	Processing method	Notes
	Nighttime lights	NL	—	Proxy indicator of economic capacity, reflecting people's ability to access cooling resources such as air conditioning
	Distance to hospital	DH	Euclidean distance	Accessibility of medical services during extreme heat
	Distance to emergency shelters	DES	Euclidean distance	Accessibility of cooling shelters in emergency situations
	Distance to commercial area	DCA	Euclidean distance	Influences residents' ability to access resources, services, and heat protection measures under high temperatures
	Distance to cultural space	DCS	Euclidean distance	
	Distance to metro station	DMS	Euclidean distance	

Note: In the formulas, BS_i is the building footprint area;BH_i is building height; S_{site} represents the plot area; $\bar{d}_i$ denotes the average distance from building i within the raster to its nearest neighboring building;S represents the impervious surface area of the sample site; $NDVI$ refers to the $NDVI$ value of pixels with bare soil cover, and $NDVI_{min}$ and $NDVI_{max}$ correspond to NDVI values at cumulative frequencies of 2% and 98%, respectively.

2.5.2 CatBoost-SHAP modeling

Subjective and objective heat exposure are jointly influenced by multidimensional factors such as land cover, urban morphology, and socioeconomic conditions; traditional linear regression methods have limitations in handling outliers, multicollinearity, and capturing complex nonlinear relationships among variables, therefore this study adopts the CatBoost model to account for nonlinear effects of urban factors on heat exposure. CatBoost is a machine learning algorithm based on gradient boosting decision trees that employs an ordered boosting strategy, which

reduces prediction bias and overfitting risk and demonstrates strong robustness in handling nonlinear relationships, multi-source heterogeneous data, and outliers(Prokhorenkova et al., 2017; Yixiao Zhang et al., 2020), the training process of gradient boosting decision trees can be expressed as:

$$F_0(x) = \mathrm{argmin}_c \sum_{i=1}^{n} \mathrm{L}\,(y_i, c) \tag{5}$$

$$F_m(x) = F_{m-1}(x) + \eta \mathrm{h}_m(x) \tag{6}$$

$$r_{im} = -\left[\frac{\partial L(y_i, F_{m-1}(x_i))}{\partial F_{m-1}(x_i)}\right] \tag{7}$$

$$\hat{\mathrm{y}} = \mathrm{F_M(x)} = \mathrm{F_0(x)} + \sum_{\mathrm{m=1}}^{\mathrm{M}} \eta\, \mathrm{h_m(x)} \tag{8}$$

Where $\mathrm{L}(\mathrm{y_i}, \mathrm{c})$ denotes the loss function, c is the initial prediction value, $\mathrm{F_m(x)}$ is the model prediction after the m-th iteration, η is the learning rate, $\mathrm{h_m(x)}$ is the decision tree trained in the m-th iteration, $\mathrm{r_{im}}$ represents the negative gradient residual, and M is the number of decision trees.

To improve model generalizability, the dataset was divided into training and testing sets at a ratio of 7:3. Five-fold cross-validation was further applied for model training and evaluation. Four machine learning models (CatBoost, XGBoost, LightGBM, and NGBoost) were evaluated, with detailed parameter settings and performance metrics reported in Appendix S2. CatBoost achieved the highest predictive accuracy among

391 the tested models and was therefore used for subsequent analysis. The
392 model performance differed between OHE and SHE, with R^2 values of
393 0.776 and 0.421, respectively. Given the relatively limited explanatory
394 power of the SHE model, the SHAP results for SHE and the mismatch
395 index D should be interpreted as association patterns under the available
396 variables rather than comprehensive mechanistic explanations.

397 However, machine learning models often suffer from the “black box”
398 problem; therefore, this study further integrates the SHAP method to
399 interpret the model results. SHAP is based on Shapley value theory in
400 game theory; by quantifying the marginal contribution of each variable to
401 model predictions, it identifies key driving factors and their directions of
402 influence and reveals nonlinear response relationships between variables
403 and heat exposure(Lundberg & Lee, 2017). The SHAP value represents
404 the contribution of factor j to the model output, and the specific formula
405 is as follows:

$$\emptyset j = \sum_{S \subseteq N \backslash \{j\}} \frac{|S|!\,(n - |S| - 1)!}{n!} \left(f(S \cup \{j\}) - f(S)\right) \tag{9}$$

406 In Equation (9), n denotes the total number of factors, N\{j}
407 represents the set of all possible factor combinations excluding j, S is a
408 subset of N\{j}, f(S) represents the model output for factors in set, and $\emptyset j$
409 denotes the contribution of variable j to the model prediction.

After model training, SHAP values were used to quantify the contribution magnitude and direction of each factor to OHE, SHE, and the mismatch index D. By comparing the differences in variable contribution patterns across these models, this study further identified the potential association patterns of objective and subjective heat exposure and their spatial mismatch.

3. Results

3.1 Spatial patterns of OHE and SHE

Based on the 0.5 and 1 standard deviation method, this study classifies OHE and SHE into five levels: low exposure, relatively low exposure, moderate exposure, relatively high exposure, and high exposure (Figure 5); the statistical results show differences in their value distributions. The median values of OHE across all levels range from 0.24 to 0.72, whereas those of SHE range from 0.12 to 0.97, indicating a larger variability in SHE values and stronger spatial heterogeneity in subjective heat exposure.

In terms of spatial distribution patterns, OHE and SHE in Xi'an exhibit different characteristics. Some core built-up areas show high objective heat exposure, but subjective heat perception does not increase correspondingly; conversely, some peripheral or open areas exhibit high

SHE despite low OHE. Overall, OHE exhibits a continuous physical thermal environment gradient, whereas SHE is more localized and dispersed, showing a certain spatial mismatch. This indicates that objective and subjective heat exposure do not exhibit a simple one-to-one correspondence, and there is a certain degree of spatial divergence between them in urban space. This difference provides a basis for subsequent LCZ-based typological analysis and identification of subjective–objective mismatch.

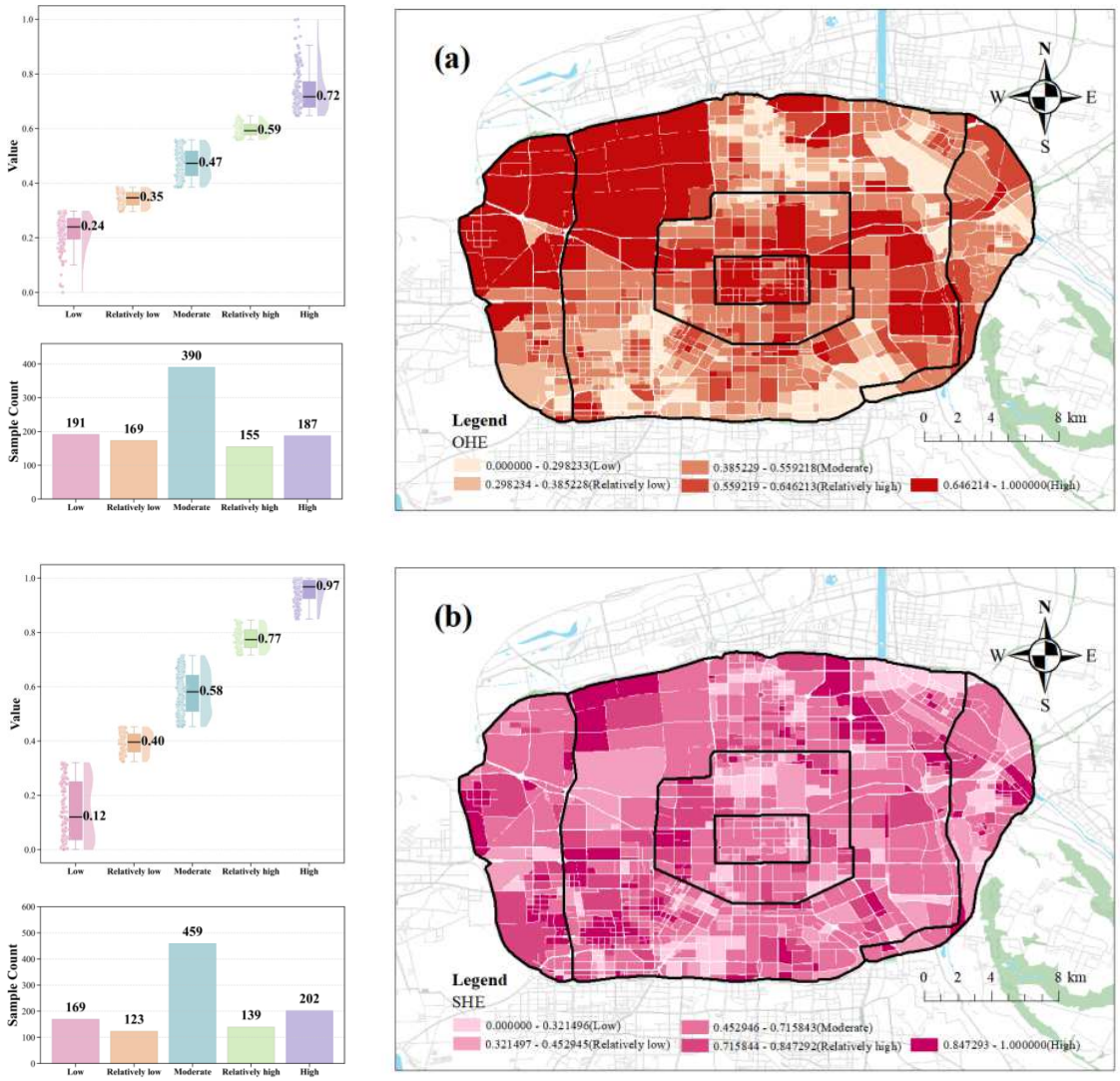


Figure 5 Heat exposure risk classification map of Xi'an: (a) objective heat exposure; (b) subjective heat exposure

3.2 Differences in OHE and SHE across different LCZ types

A total of 1,082 LCZ sample units were delineated in the study area, covering a total area of 400.93 km², with a classification accuracy of 87.5%, meeting the requirements for subsequent analysis (Figure 6, Table 5). Among them, built types (LCZ1–8) account for 77% of the units, while land cover types (LCZA–D) account for 23%. LCZ4 has the highest proportion at 35%, mainly distributed between the first and third ring roads; LCZD has the lowest proportion at only 1%, concentrated in the river areas in the eastern part of the study region. Overall, the LCZ spatial pattern in the study area exhibits a ring-shaped structure dominated by built types, with a clear distinction between built-up areas and natural land cover areas.

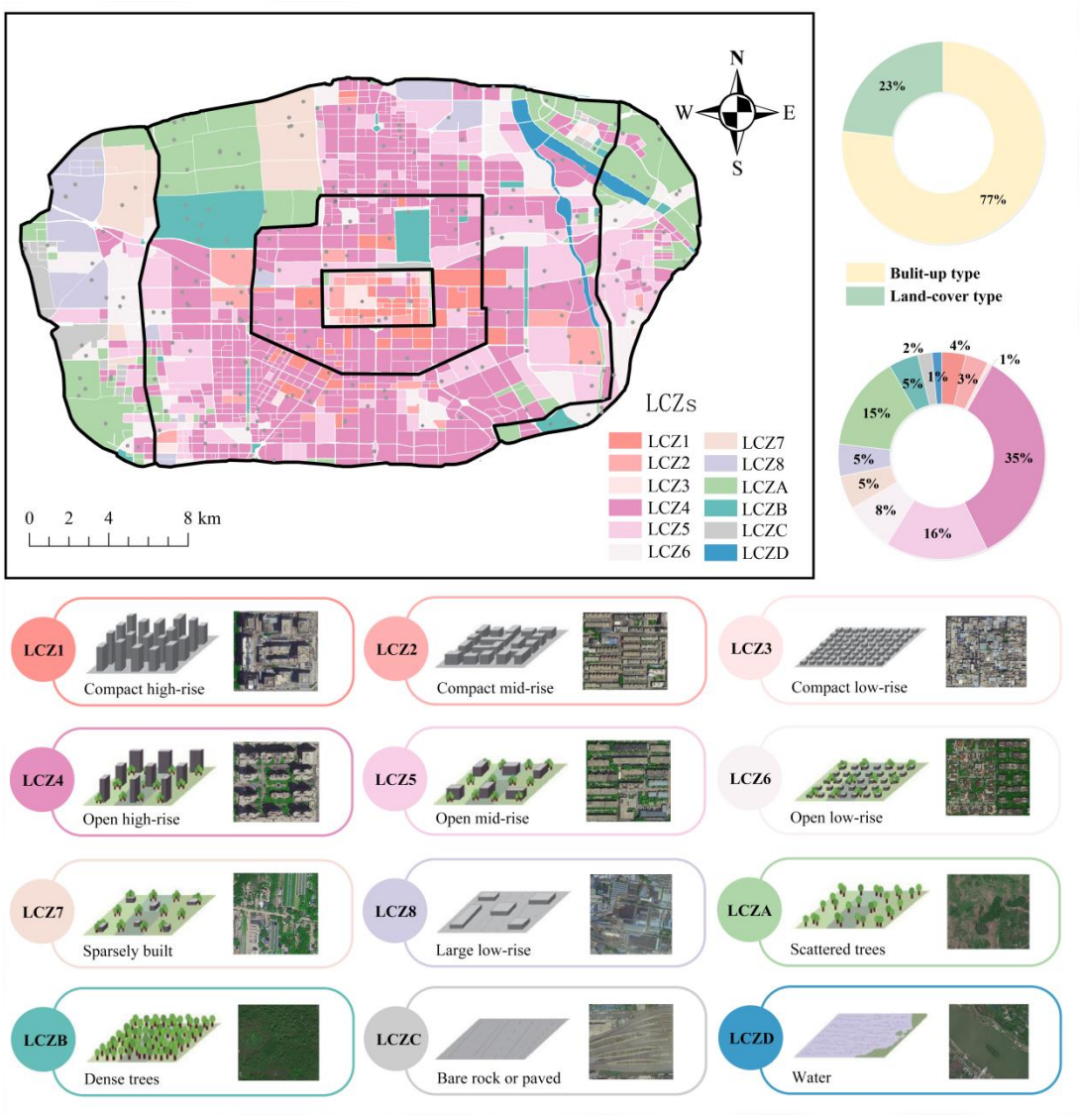


Figure 6 LCZ classification map of Xi'an

Table 5 Statistical data of LCZ zoning types in Xi'an

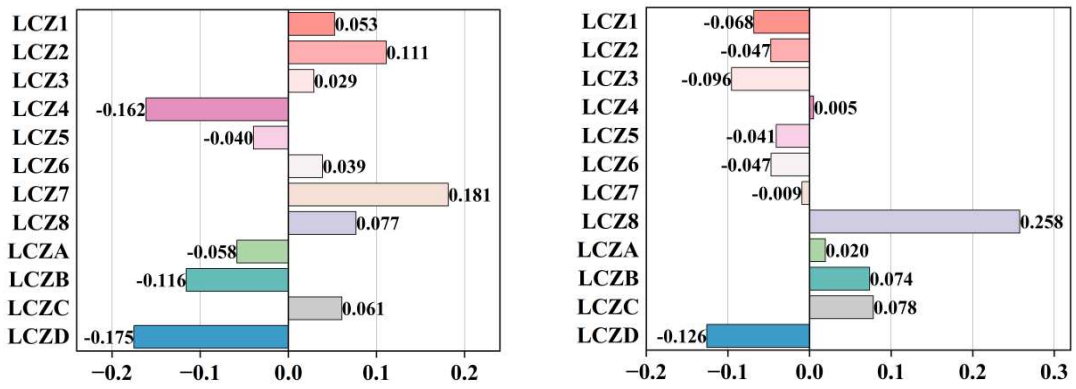
LCZ	Total number	Total area（km^2）	Average area（km^2）	Number of validation points	Accuracy rate（%）
LCZ1	52	15.12	0.29	6	66.7%
LCZ2	35	14.30	0.41	11	72.7%

LCZ	Total number	Total area（km^2）	Average area（km^2）	Number of validation points	Accuracy rate（%）
LCZ3	12	3.30	0.28	2	100%
LCZ4	532	138.77	0.26	53	90.5%
LCZ5	140	64.19	0.46	39	89.7%
LCZ6	78	31.10	0.40	28	85.7%
LCZ7	16	21.18	1.32	8	75%
LCZ8	7	20.07	2.87	4	75%
LCZA	128	59.40	0.46	29	93.1%
LCZB	30	18.51	0.62	9	100%
LCZC	38	8.97	0.24	9	77.8%
LCZD	14	6.02	0.43	2	100%
Total	1082	400.93	0.37	200	OA=87.50% Kappa=0.852

The deviations between OHE and SHE across different LCZ types exhibit significant differences (Figure 7). High OHE deviations are mainly concentrated in LCZ1–3 and LCZ7, while low deviations occur in LCZ4, LCZB, and LCZD, with LCZD exhibiting the most pronounced cold island effect. In contrast, the spatial distribution pattern of SHE differs markedly from that of OHE; LCZ types with high SHE deviation include LCZ8, LCZC, and LCZB, while LCZD exhibits the weakest

460 subjective heat perception, and most built-type LCZs show negative SHE
461 deviations.

462 Overall, different LCZ types show clear spatial differentiation
463 between OHE and SHE; some LCZ types exhibit high OHE but low SHE,
464 while others show higher SHE than OHE. This indicates that relying
465 solely on objective thermal environment indicators is insufficient to fully
466 capture differences in perceived heat risk among residents. The spatial
467 differences between OHE and SHE provide a basis for subsequent
468 LCZ-based mismatch classification analysis and offer a visual reference
469 for differentiated heat environment management.



（a）OHE （b）SHE

Figure 7 Deviations in two types of heat exposure across different LCZ types

470 To further identify the relationship between OHE and SHE, this
471 study constructs a four-quadrant analytical framework based on the
472 relative deviations of OHE and SHE across LCZ types (Figure 8). Using

zero as the reference for the overall study-area mean, LCZ types are classified into four categories of subjective–objective heat exposure relationships: high OHE–low SHE, high OHE–high SHE, low OHE–high SHE, and low OHE–low SHE.

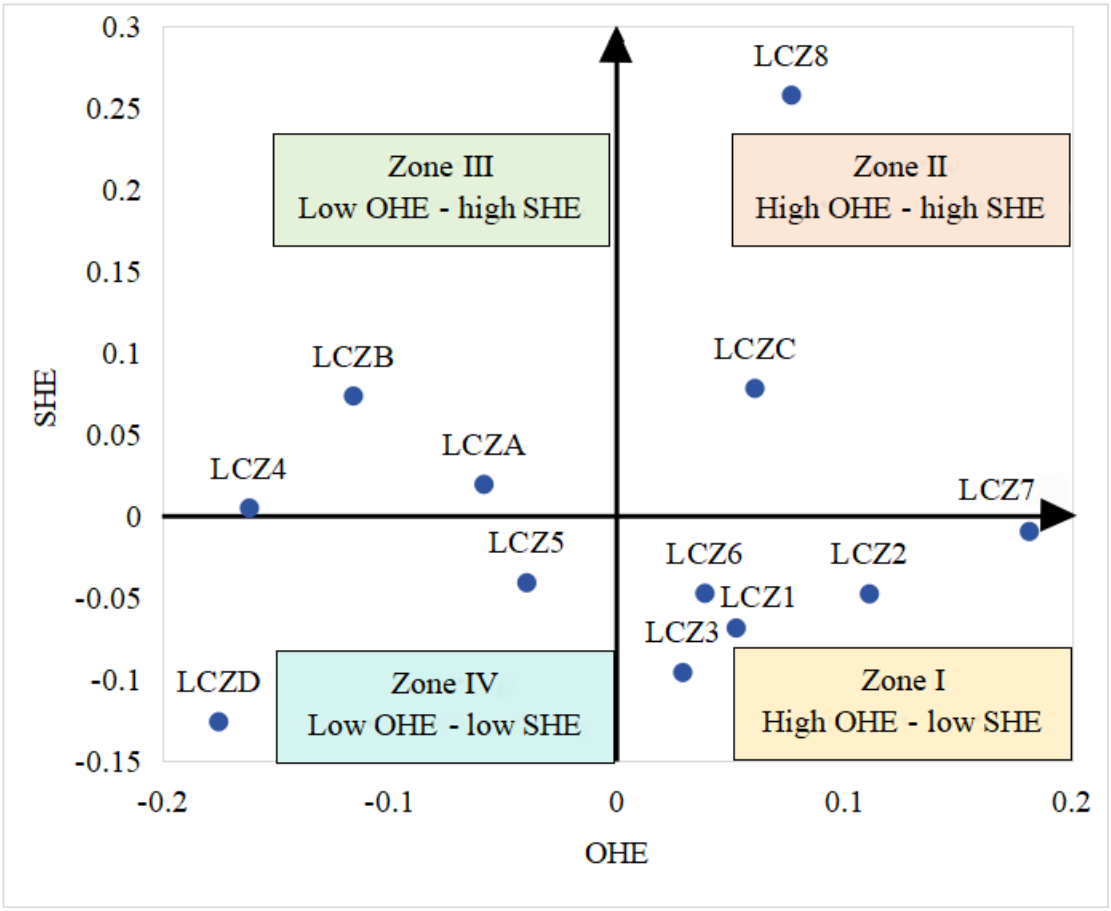


Figure 8 Four-quadrant distribution of OHE–SHE mean deviations based on LCZ.

The results show that LCZ1, LCZ2, LCZ3, LCZ6, and LCZ7 mainly exhibit high OHE and low SHE, indicating that subjective thermal discomfort does not increase correspondingly in some high-temperature built environments. LCZ8 and LCZC exhibit both high OHE and high

SHE, representing key areas where objective heat risk and subjective thermal discomfort co-occur.LCZ4, LCZA, and LCZB mainly show low OHE and high SHE, suggesting that low physical thermal exposure does not necessarily correspond to low subjective thermal discomfort. LCZ5 and LCZD exhibit both low OHE and low SHE, representing areas where objective and subjective thermal environments are relatively consistent.

Overall, the High OHE–Low SHE and Low OHE–High SHE categories reflect typical mismatches between OHE and SHE and represent two key spatial types that are easily overlooked under a single physical temperature-based evaluation framework. This finding further indicates that jointly considering OHE and SHE within the LCZ framework helps identify spatial differences in heat risk that cannot be captured by a single objective temperature indicator, highlighting the need for further analysis of their formation mechanisms and governance implications.

3.3 Differences in driving factors of subjective–objective heat exposure and their mismatch

Multicollinearity among the input variables was systematically assessed using Pearson correlation analysis and the variance inflation factor (VIF) (Fig. 9). The results showed that several urban morphological variables exhibited moderate correlations consistent with

their physical relationships. For example, building proximity (PROX) was negatively correlated with sky view factor (SVF) (r = −0.69), while building density (BD) showed a positive correlation with impervious surface fraction (ISF) (r = 0.70). However, all variables had VIF values below the commonly used threshold of 5, indicating no severe multicollinearity among the predictors. Considering the robustness of CatBoost in handling correlated predictors, the subsequent SHAP-based interpretation provided a reliable basis for identifying the relative contributions and nonlinear effects of different factors.

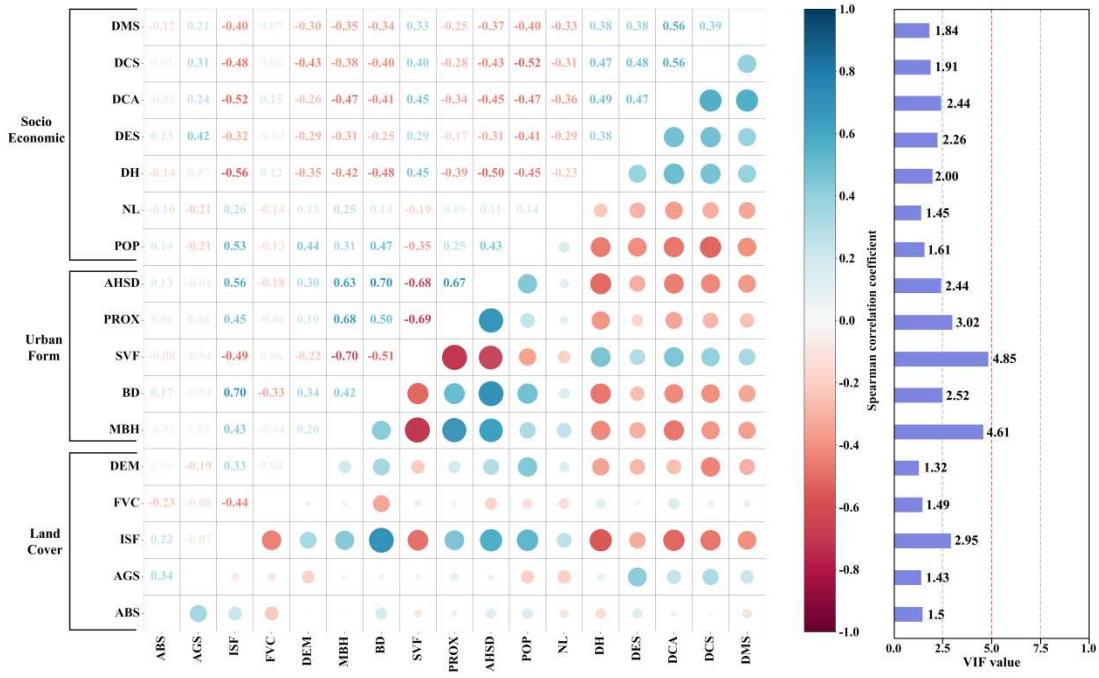


Figure 9 Pearson correlation matrix of selected predictor variables in the CatBoost model

As shown in Figure 10, the relative importance of the factors associated with OHE and SHE differs substantially.For OHE, urban morphology factors make the largest contribution (39.1%), followed by land-cover factors (31.1%), whereas socioeconomic factors make a relatively smaller contribution (27.6%).This indicates that OHE is mainly associated with building form, land cover, and physical thermal conditions.By contrast, the factor structure of SHE is more diverse: socioeconomic factors make the largest contribution (38.6%), land-cover factors account for 34.3%, and the contribution of urban morphology factors decreases to 16.8%.In addition, the interaction contribution associated with OHE in the SHE model is 10.4%, suggesting that OHE is associated with subjective thermal perception but is not its sole explanatory factor.

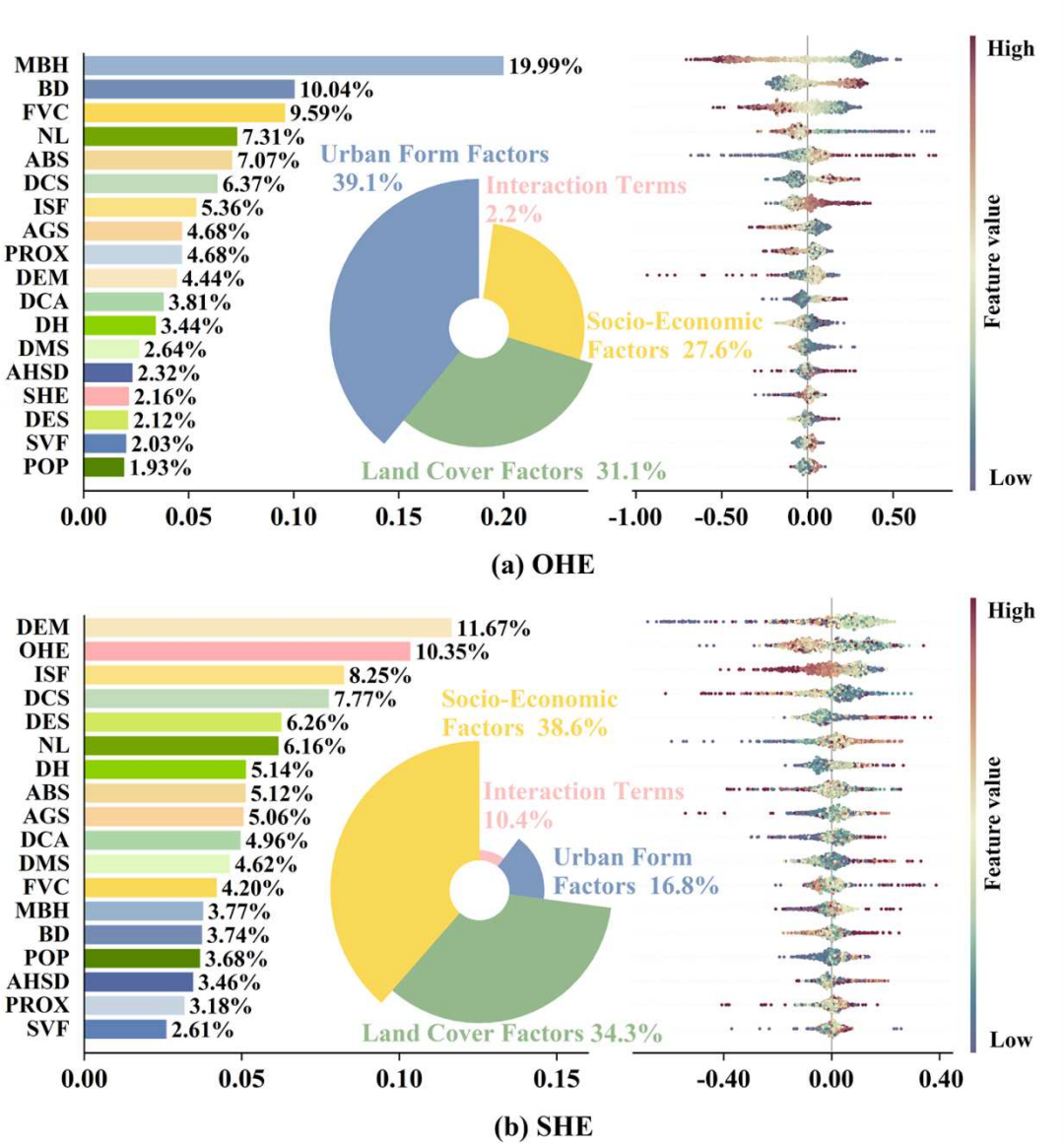


Figure 10 Comparison of the importance of driving factors for OHE and SHE: (a) feature importance ranking and influence direction of OHE; (b) feature importance ranking and influence direction of SHE.

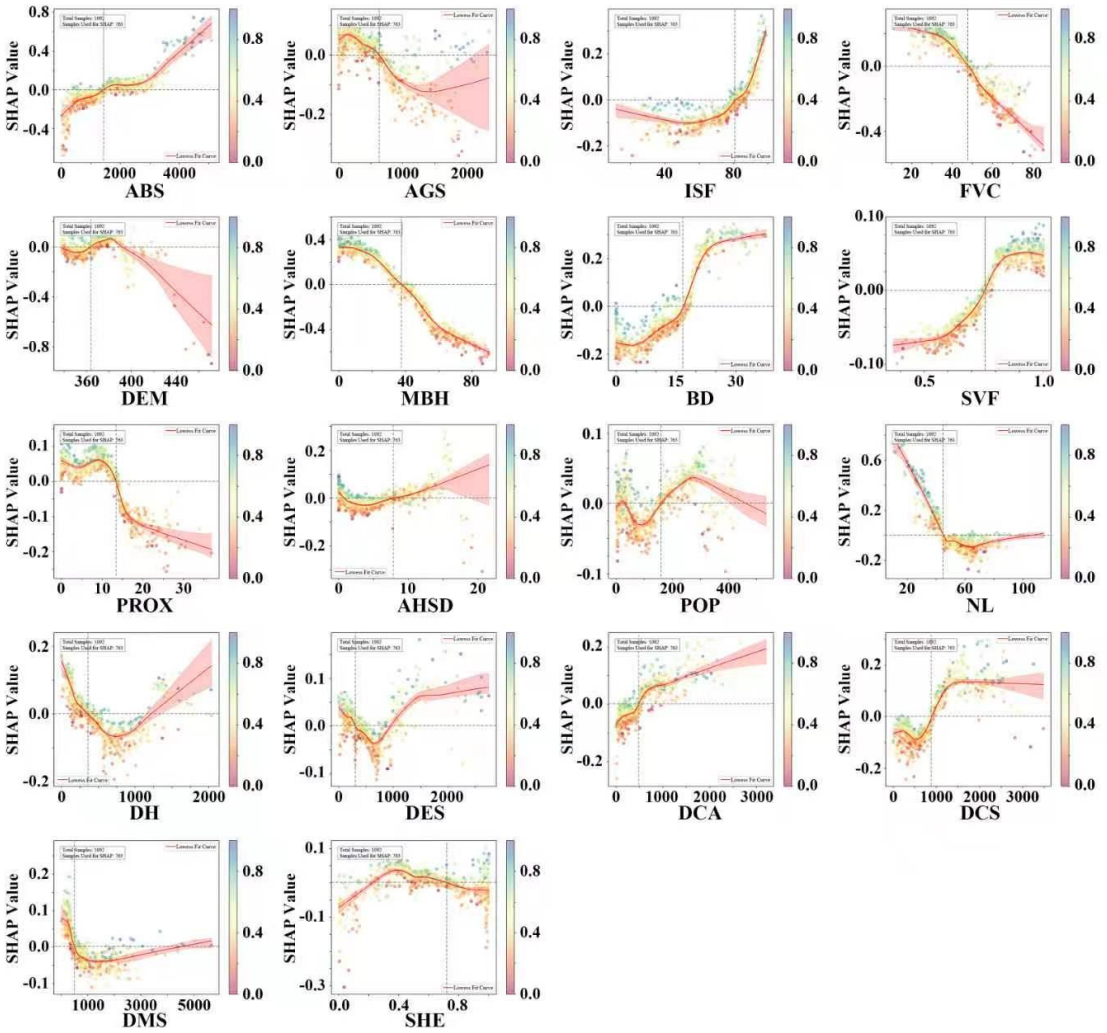
The local SHAP dependence results indicate that the factors associated with OHE and SHE can be divided into two patterns (Figures 11 and 12).

Factors with consistent directions but different thresholds: SVF, BD, AHSD, and DCA all show positive contributions in both models, but their critical points for changing from negative to positive differ.For example, the positive turning point of SVF is approximately 0.75 in the OHE model but is delayed to 0.90 in the SHE model, indicating that subjective thermal perception has a higher response threshold to spatial openness.

Factors with inconsistent directions: ISF, MBH, and FVC exhibit inconsistent or even opposite responses in the two models.When ISF exceeds 80%, it is positively associated with OHE but negatively associated with SHE.MBH is generally negatively associated with OHE, with a stronger effect above 35 m, but is positively associated with SHE.FVC is negatively associated with OHE above 45%, whereas its direction of association with SHE is unclear and shows only a weak negative association in the 50%–70% range.In addition, the estimated effect of OHE on SHE is nonlinear: it is positive in the 31–34 °C range and above 38 °C, but becomes negative in the 34–38 °C range.

These direction-reversing factors, such as ISF and FVC, correspond closely to the two mismatch categories identified in the LCZ four-quadrant framework.Built-up areas with high ISF are more likely to exhibit High OHE–Low SHE, whereas open and vegetated areas with low ISF and high FVC are more likely to exhibit Low OHE–High

559 SHE.This provides a factor-level explanation for the spatial patterns
560 reported in Section 3.2.



561

562 Figure 11 Local SHAP effects of OHE features

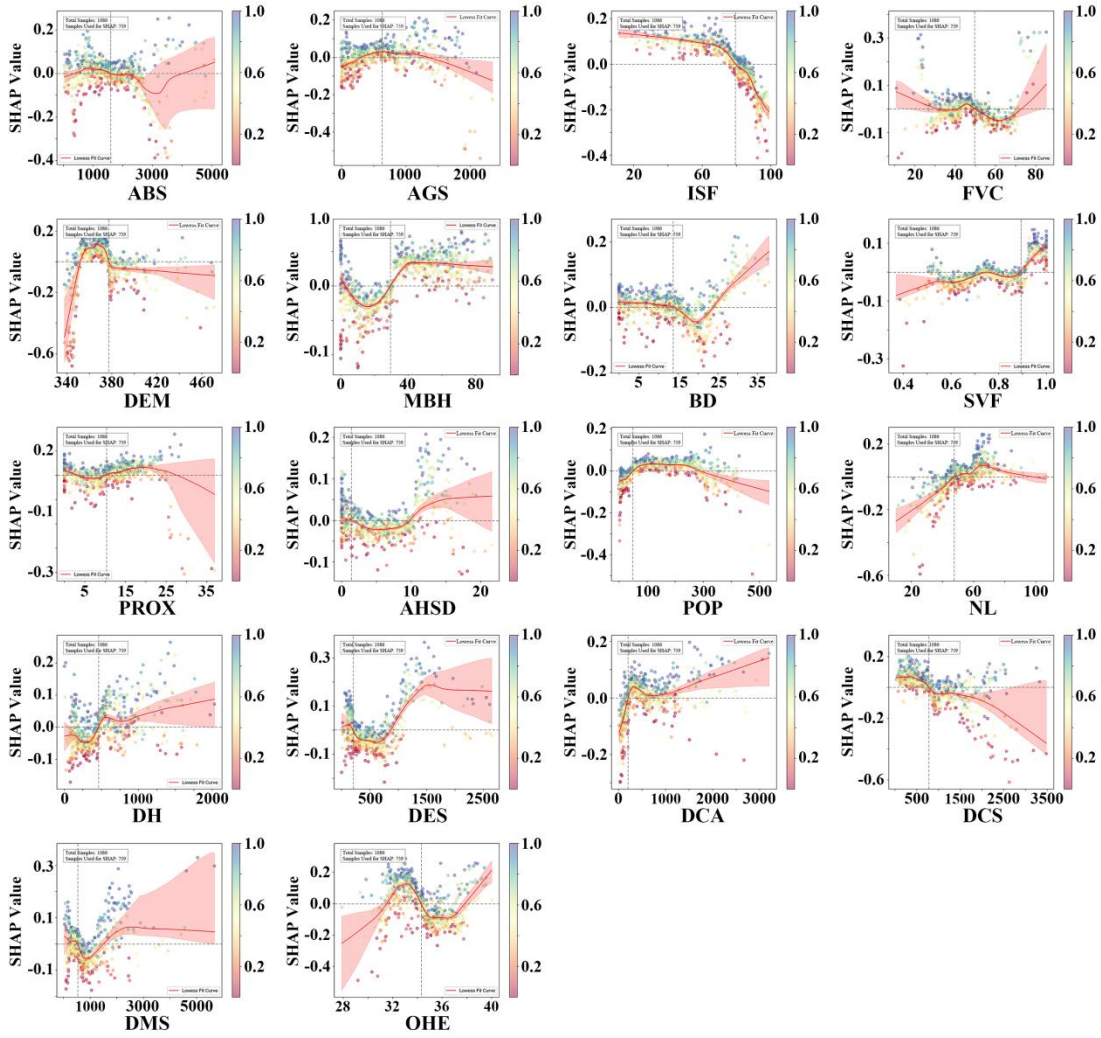


Figure 12 Local SHAP effects of SHE features

To further identify the factors associated with deviations between OHE and SHE, this study constructed the mismatch index D and developed separate models for the two mismatch categories: High OHE – Low SHE (LCZ1, LCZ2, LCZ3, LCZ6, and LCZ7) and Low OHE – High SHE (LCZ4, LCZA, and LCZB) (Figures 13 – 15).In both mismatch categories, D is most strongly associated with the socioeconomic and land-cover dimensions; the socioeconomic dimension

ranks first in both categories, accounting for 44.6% and 38.1%, respectively.However, the specific key factors differ.The three most important factors in the High OHE－Low SHE areas are DES (18.36%), NL (14.93%), and ABS (14.29%), whereas those in the Low OHE－High SHE areas are DEM (12.76%), DH (9.38%), and DCS (7.98%).

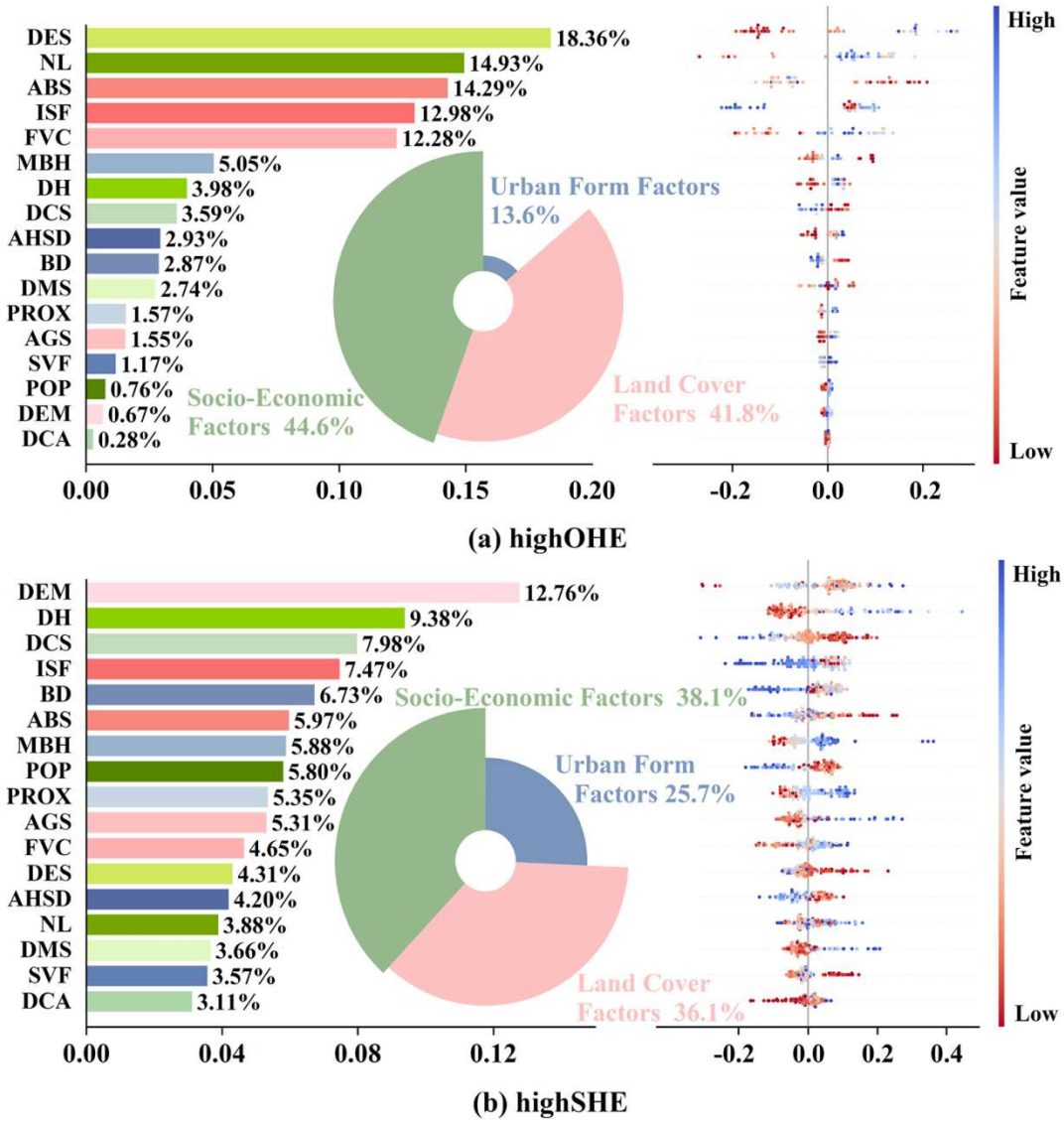


Figure 13 Comparison of the importance of driving factors of D: (a) feature importance ranking and influence direction of D in High OHE–

Low SHE areas; (b) feature importance ranking and influence direction of D in Low OHE–High SHE areas.

The local SHAP effects further reveal the association patterns of individual factors in the two mismatch categories.Most factors have consistent directions of association, suggesting that the mismatch may have some common correlates.Higher FVC values and lower ISF, ABS, and DCS values are associated with positive SHAP contributions to D in both categories, indicating that areas with greater natural cover or shorter distances to water bodies and cultural facilities cannot simply be assumed to have smaller deviations between objective and subjective heat exposure.Lower AGS, DH, and DCA values are likewise associated with negative SHAP contributions to D in both categories; that is, areas closer to parks, hospitals, and commercial facilities tend to show smaller deviations.This suggests that access to activity opportunities and cooling resources may help alleviate the mismatch.However, some factors have different directions of association across the two mismatch categories.The standard deviation of building height (AHSD), population density (POP), and distance to emergency shelters (DES) show opposite effects.High AHSD, POP, and DES are positively associated with D in High OHE – Low SHE areas but negatively associated with D in Low OHE – High SHE areas, indicating that their associations with D vary across mismatch contexts.

Overall, variation in D in both mismatch categories is jointly associated with land cover, urban morphology, and socioeconomic factors.Although most factors show common effects across mismatch types, the divergent directions of AHSD, POP, and DES indicate that the association pattern of the mismatch is not uniform but varies according to context.

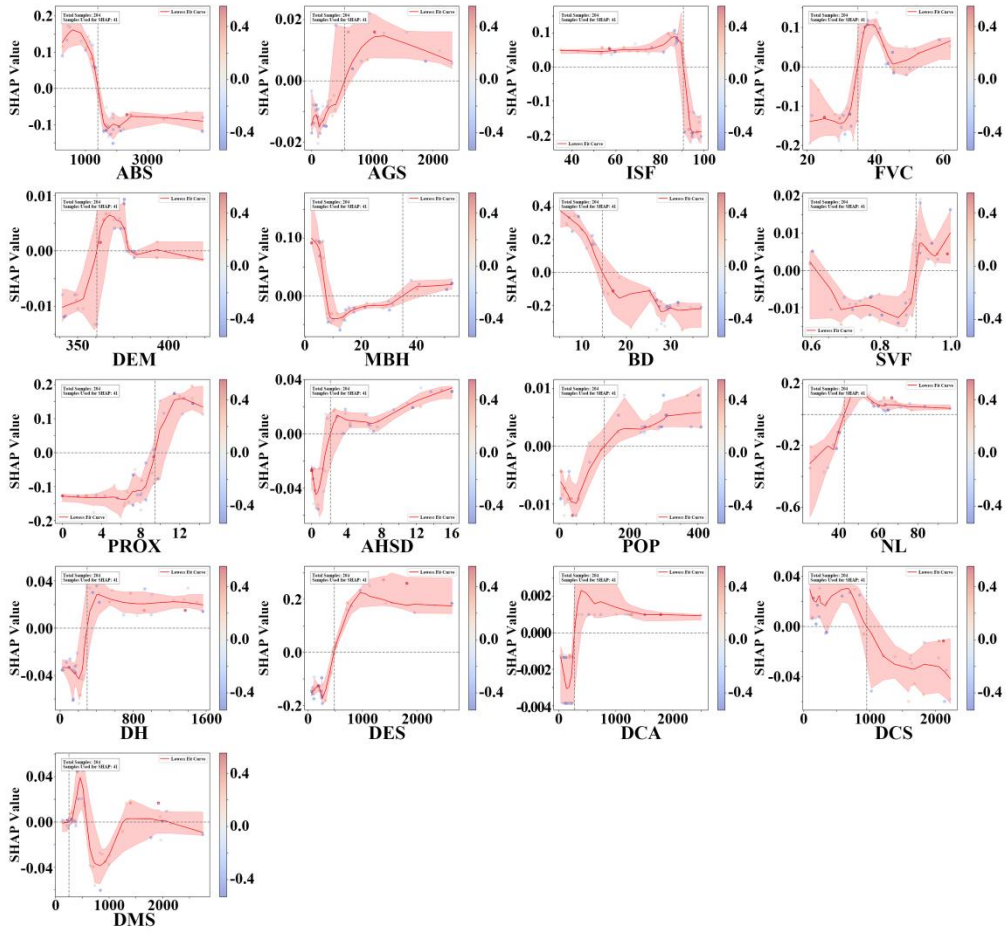
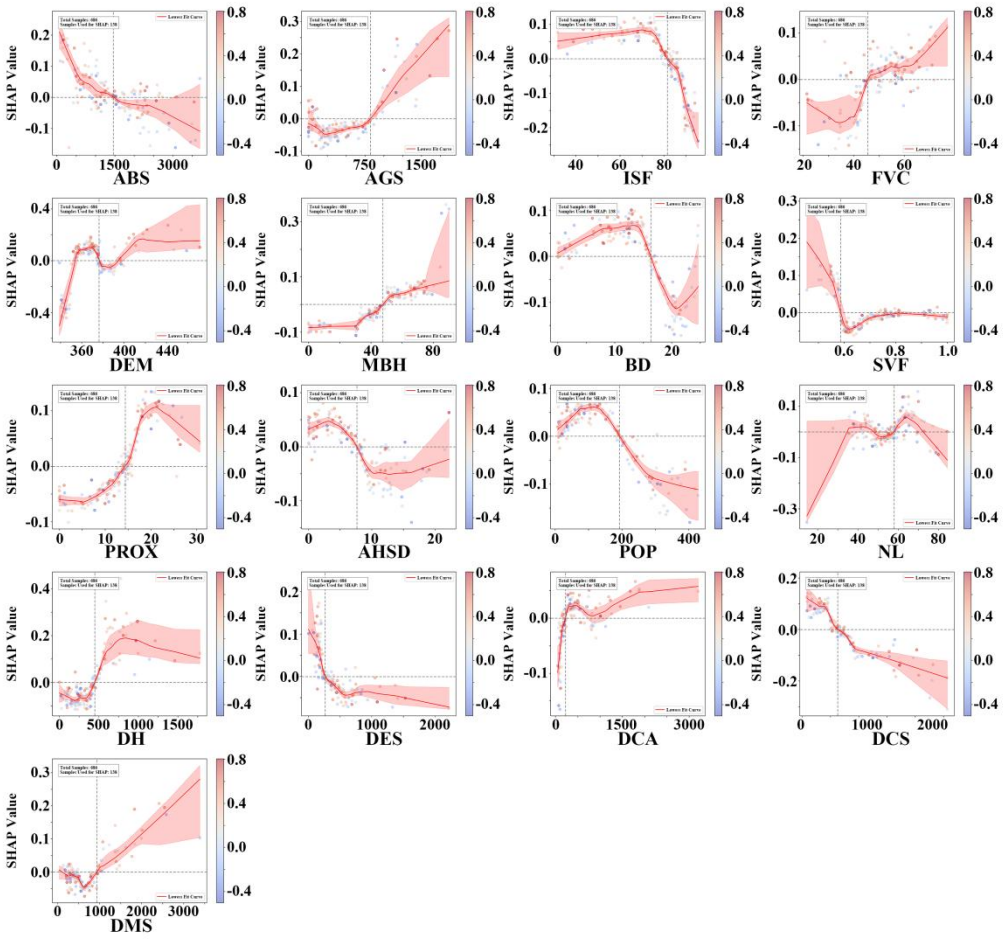


Figure 14 Local SHAP effects of D features in High OHE–Low SHE areas



611

612 Figure 15 Local SHAP effects of D features in Low OHE–High SHE

613 areas

614 ## 4. Discussion

615 ### 4.1 Spatial mismatch patterns of OHE and SHE

616 This study yielded the following findings concerning OHE, SHE,

617 and their spatial relationship.

First, the spatial pattern of OHE is consistent with established findings from conventional urban thermal-environment research. Most built LCZ types show higher OHE, whereas natural LCZ types (LCZA, LCZB, and LCZD) generally exhibit lower OHE. Compact built types tend to have greater heat exposure than open built types, suggesting that LCZs can effectively characterize spatial variations in urban thermal conditions. Similar patterns have been reported in different cities and climate contexts (Table 6). In this study, LCZ4 had the lowest OHE among built types, consistent with previous findings for Xi’an based on enhanced LST data(Han et al., 2023).The relatively high OHE of LCZ7 may be related to its limited samples and the concentration of the study area within the Third Ring Road. These results confirm the suitability of the LCZ framework for analyzing OHE patterns, while previous LCZ studies have rarely examined the mismatch between objective thermal conditions and subjective heat perception.

Table 6 compares studies of summer objective thermal environments conducted within the LCZ framework.

Author	Study city	Data source	Main findings
Han et al.(Han et al., 2023)	Xi'an	Land surface temperature	Compact mid-rise buildings (LCZ2) had the highest temperature, whereas open high-rise buildings (LCZ4) had the lowest.
Huo et al.(Hou et al., 2023)	Shanghai	Land surface temperature	Mean daytime LST in compact mid-rise, compact low-rise, large

Author	Study city	Data source	Main findings
			low-rise, and heavy-industry areas was higher than that in other LCZ types.
Wang et al.(R. Wang et al., 2024)	Chongqing	Land surface temperature	Natural LCZ types generally had lower temperatures than built LCZ types.
Yang et al.(Xiang et al., 2023)	Wuhan, Nanjing, and Shanghai	Land surface temperature	High-density built LCZs were associated with high-temperature areas, whereas natural LCZs were associated with lower thermal intensity.
Li et al.(Li et al., 2021)	Three major urban agglomerations in China	Land surface temperature	Compact built LCZs had higher heat intensity, whereas natural LCZs had a stable cooling effect.
O'Malley et al.(O'Malley & Kikumoto, 2022)	Tokyo	Land surface temperature	Compact low-rise areas had higher LST, whereas natural LCZs had a marked cooling effect.
Koth et al.(Kotharkar et al., 2024)	Nagpur	In situ meteorological data	Compact built LCZs had greater heat stress than open and vegetated LCZs.
Núñez-Peiró et al.(Núñez-Peiró et al., 2021)	Madrid	Air temperature	Heat accumulation was stronger in densely built areas than in natural areas.

To address this gap, this study further identified the spatial mismatch between SHE and OHE within the LCZ framework.The level of objective heat exposure does not fully determine the level of subjective heat exposure: areas with high OHE, such as LCZ1, LCZ2, LCZ3, LCZ6, and LCZ7, do not necessarily correspond to high SHE, whereas areas with low OHE, such as LCZ4, LCZA, and LCZB, may correspond to high SHE.The two measures show opposite response patterns in some spatial types, and temperature hotspots only partially overlap with hotspots of subjective thermal perception.Previous studies also suggest this possibility: residents' subjective thermal perception is not a linear

function of objective temperature but is jointly regulated by individual adaptive capacity and environmental details (Gu et al., 2026; Shooshtarian et al., 2017), as well as socioeconomic conditions and access to resources (Guo et al., 2025; Lee & Han, 2024; Zeng et al., 2022b).In addition, studies based on social media, questionnaires, and field measurements have confirmed similar deviations from different perspectives (Table 7), providing cross-case evidence for the findings of this study.A further contribution of this study is to use LCZs to systematically associate the direction and spatial organization of these deviations with specific urban spatial types.In this way, LCZs are extended from a tool for classifying objective thermal environments to a spatial-context framework for organizing the relationship between objective and subjective heat exposure, addressing the relatively limited characterization of subjective heat exposure in LCZ research.The two mismatch categories represent different types of risk.Low OHE – High SHE areas have relatively low objective temperatures but strong subjective thermal perception and may easily be overlooked because they do not appear on temperature-hotspot maps.Although High OHE – Low SHE areas exhibit relatively low subjective thermal perception, previous studies have shown that long-term heat adaptation can alter residents' thermal perception but cannot eliminate the physiological heat burden caused by sustained high-temperature exposure (Gasparrini et al.,

667 2015).Lower risk perception may also reduce residents' willingness to
668 take protective actions, making these areas potential units of
669 underestimated risk (Heidenreich & Thieken, 2024; Beckmann et al.,
670 2021).Together, the two categories constitute governance blind spots
671 under conventional temperature-hotspot assessment frameworks.

672 Table 7 compares studies reporting inconsistencies between subjective
673 perception and objective indicators.

Author	Study city	Data source	Main findings
He et al.(He et al., 2025)	Chengdu	Thermal perception derived from social-media text + land surface temperature	Systematic differences exist between objective and subjective heat exposure.
Liu et al.(Qiqi Liu, Tian %J Sustainable Cities Hang, et al., 2025)	Beijing	Thermal perception derived from social-media text + land surface temperature	Objective and subjective heat exposure differ substantially, indicating a perceptual gap between thermal perception and objective conditions.
Zhang et al.(Zhang et al., 2026)	Beijing	Thermal perception derived from social-media text + land surface temperature	A significant spatial mismatch exists between SMHP and PTE, challenging the conventional assumption that PTE adequately represents residents' thermal experiences.
Peng et al.(Peng et al., 2022)	Rome	Questionnaire, wearable physiological sensors + measured meteorological data	Subjective thermal perception deviated significantly from objective UTCI and skin temperature.
Schaefer et al.(Schaefer et al., 2021)	Dortmund	Questionnaire + measured meteorological data	The objective–subjective mismatch showed a dependence on spatial direction.
Li et al.(Li et al., 2022)	Guangzhou	Questionnaire + measured meteorological data	Objective indicators systematically underestimated residents' actual experiences.
Sánchez Ramos et al.(Sánchez Ramos et al., 2022)	Seville	Questionnaire + measured meteorological data	The COMFA model systematically overestimated outdoor thermal discomfort, and the range of residents' actual comfort was approximately 60% wider than the model prediction.

Author	Study city	Data source	Main findings
Xie et al.(Xie et al., 2022)	Beijing	Questionnaire + measured meteorological data	The same objective thermal environment produced significantly different subjective thermal evaluations because the order of heat-exposure sequences differed.
Ning et al.(Ning et al., 2023)	Xi'an	Questionnaire + measured meteorological data	At the same objective UTCI level, subjective thermal sensations diverged systematically because of differences in perceived sunlight exposure.

In summary, this study further identifies two spatial types that have rarely been systematically distinguished: areas where objective temperatures are high but residents' perceptions are weak, and areas where objective temperatures are not high but residents' perceptions are strong.OHE reflects potential physical heat exposure, whereas SHE reflects observable subjective-perception responses; the two are not equivalent, and their correspondence and divergence together provide a more complete spatial representation of urban heat risk.This study extends the conventional temperature-hotspot framework for heat-risk assessment and provides a basis for accurately identifying governance blind spots and formulating differentiated intervention strategies in urban thermal-environment management.

4.2 Association patterns between urban environmental factors and objective–subjective heat-exposure mismatch

The CatBoost–SHAP analysis further identified factor patterns associated with objective–subjective heat-exposure mismatch.The

mismatch pattern was not linked to a single environmental factor; rather, it was associated with inconsistent response pathways involving the physical thermal environment, residents' perceptual responses, and heat-adaptation conditions.Unlike existing analytical frameworks that examine factors associated with OHE or SHE separately (He et al., 2025), this study simultaneously compares the association structures of OHE, SHE, and their deviation, D, thereby further revealing differentiated response patterns of objective and subjective heat exposure in urban space.

First, OHE and SHE exhibit distinct factor-response structures.OHE is mainly associated with physical environmental factors such as urban morphology and land cover, among which mean building height (MBH), building density (BD), and fractional vegetation cover (FVC) are important explanatory variables; this is broadly consistent with previous local research in Xi'an (C. Wang et al., 2024).By contrast, SHE and its deviation from OHE exhibit more complex association patterns and are associated not only with the physical environment but also with socioeconomic factors.This indicates that residents' thermal perception is not a direct mapping of objective heat exposure but is jointly shaped by activity spaces, access to resources, and heat-adaptation conditions on the basis of the physical environment.Accordingly, the same environmental factor may be associated with OHE and SHE in different or even opposite

712 directions.For example, FVC makes a stable negative contribution to
713 OHE, but its effect on SHE is not fully consistent.This is consistent with
714 the finding reported by He et al. (He et al., 2025) that areas with high
715 NDVI in Chengdu were associated with lower OHE but did not
716 necessarily produce a corresponding reduction in subjective thermal
717 perception because of insufficient shading.Similarly, the sky view factor
718 (SVF) makes positive contributions to both OHE and SHE, with
719 thresholds of 0.75 and 0.90, respectively.This may reflect the effect of
720 increased spatial openness on solar-radiation exposure (Song et al., 2025)
721 and indicates that subjective thermal perception may respond to spatial
722 openness only under stronger solar-radiation exposure.The impervious
723 surface fraction (ISF) further illustrates this difference: higher ISF values
724 are associated with higher OHE but with negative SHAP contributions to
725 SHE and D.One possible explanation is that although highly built-up
726 areas intensify surface heat storage (Bai et al., 2025; Zhao et al., 2025),
727 their spatial functions and built environments may provide residents with
728 more opportunities to avoid heat, thereby weakening their direct
729 perception of the external thermal environment (Zhang et al., 2022).This
730 association pattern is consistent with the High OHE – Low SHE
731 characteristics observed in several built LCZs, particularly compact built
732 types, indicating that greater physical heat exposure in highly built-up
733 environments does not necessarily translate into stronger subjective

thermal perception.Conversely, although open spaces and green areas can reduce heat exposure at the regional scale, greater solar-radiation exposure may strengthen residents' perceptual responses to local thermal-environment changes and may therefore more often result in Low OHE – High SHE.

Second, access to heat-mitigation resources plays an important role in explaining deviations between objective and subjective heat exposure.The SHAP results show that shorter distances to parks (AGS), healthcare facilities (DH), and commercial facilities (DCA) make negative contributions to D in both mismatch categories and can reduce the deviation between objective and subjective heat exposure.This indicates that urban heat risk depends not only on the thermal environment to which residents are exposed but also on whether they can obtain effective cooling and adaptation support.Previous studies have shown that urban green spaces can improve local thermal environments and reduce residents' heat stress through evapotranspiration and shading (Wang et al., 2025); meanwhile, access to cooling centers and healthcare facilities is important for improving emergency adaptive capacity during heat events (Wang et al., 2025; Nayak et al., 2019).This is consistent with the occurrence of high SHE in some areas with low OHE.Even when land surface temperature is low at the regional scale, subjective thermal perception may remain high if residents' activity spaces lack effective

shade, resting spaces, or heat-adaptation resources.However, the effects of heat-mitigation resources are not fully consistent.For example, increasing distance to water bodies (ABS) is associated with a negative SHAP contribution to D; equivalently, lower ABS values are associated with positive contributions, indicating that areas closer to water bodies may exhibit larger objective – subjective deviations.One possible explanation is that although water bodies can reduce land surface temperature through evaporative cooling (Fricke & Kabisch, 2026), they may also increase air humidity, and higher humidity reduces the efficiency of human evaporative heat loss (Hu & Li, 2020).This may offset part of the improvement in thermal comfort, although the association may also be jointly influenced by land use and human activities around water bodies.Furthermore, the group-specific models show that mismatch association patterns are strongly context-dependent.Some factors reverse direction across mismatch types.For example, distance to emergency shelters (DES) reduces D in Low OHE – High SHE areas but has the opposite effect in High OHE – Low SHE areas.This suggests that the direction of the association between a spatial factor and heat risk may vary with spatial context, indicating that residents' heat adaptation may depend on specific spatial conditions.

In summary, OHE is primarily associated with physical factors such as urban morphology and land cover, whereas SHE and its degree of mismatch with OHE are more strongly associated with socioeconomic factors and access to heat-mitigation facilities.This indicates that SHE is not a simple linear mapping of OHE and that thermal-environment governance should incorporate facility accessibility into comprehensive planning rather than rely solely on physical cooling measures.

4.3 From temperature hotspots to objective–subjective heat mismatch: a transferable diagnostic framework

Conventional urban heat-risk assessments generally use physical indicators such as LST to identify high-temperature areas and then infer their potential heat risks, implicitly assuming consistency between physical heat exposure and residents' thermal perception.However, this study finds that the two are not fully aligned.Some built LCZ types exhibit relatively high OHE but relatively low SHE, whereas some open or green LCZ types exhibit relatively low OHE but relatively high SHE.This indicates that a single temperature indicator may overlook areas with objective–subjective heat-risk mismatch. The value of incorporating subjective information therefore lies not simply in adding another heat indicator to conventional thermal maps, but in explicitly

identifying where physical and perceptual signals converge or diverge and whether such divergence is systematically associated with particular urban spatial contexts.

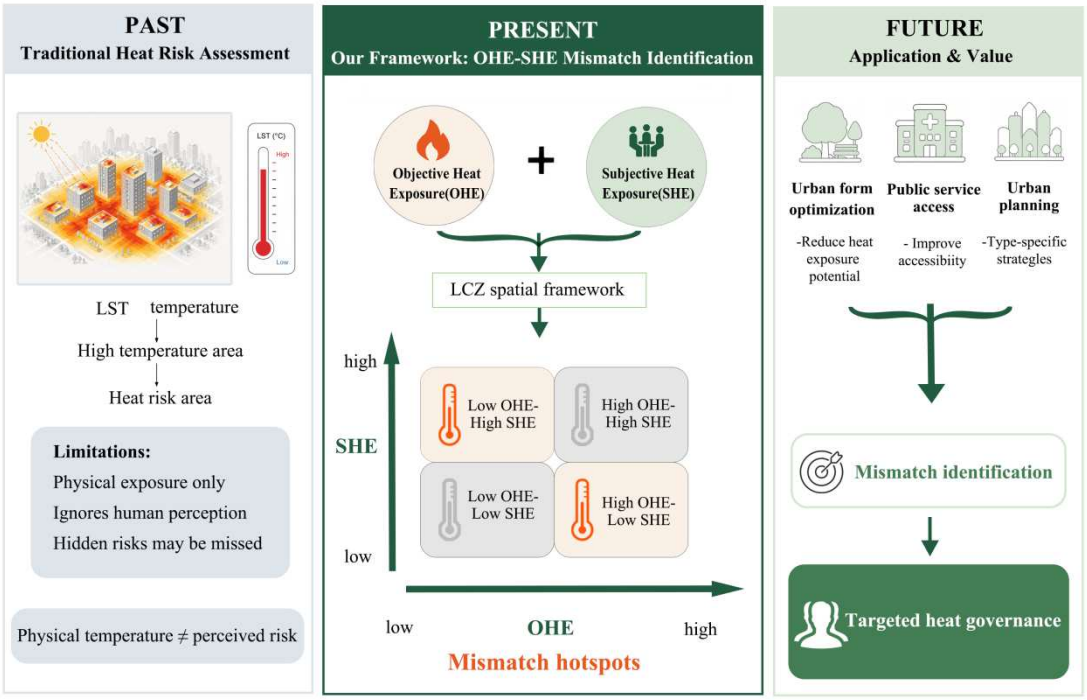


Figure 16 Analytical framework from temperature-hotspot identification to mismatch identification

To address this limitation, this study developed a two-dimensional OHE–SHE assessment system based on LCZs as unified spatial units and identified four spatial categories. This shifts the research question from "where are objective temperatures high?" toward "where do physical and perceptual heat signals correspond, and where do they diverge?" It also reveals the combined roles of the physical environment

and resource accessibility underlying these patterns.The framework extends urban heat-risk assessment from conventional temperature-hotspot identification to coordinated analysis of objective exposure, residents' perceptions, and spatial adaptation resources, providing a new analytical pathway for precise, human-centered heat governance (Figure 16).

The analytical logic of this framework can be adapted to the characteristics of individual cities.For example, this study finds that areas closer to water bodies in Xi'an do not exhibit smaller objective–subjective deviations; this association may differ in coastal cities or cities with dense river networks and higher humidity.Accordingly, humidity, sea-breeze direction, and other factors could be added to the set of variables associated with SHE in such cities.In some small and medium-sized cities, platform data from social media may be relatively sparse, and SHE could instead be constructed using questionnaires, wearable devices, or mobile-sensing data.In denser and more heterogeneous tropical cities, building forms and land uses may be more mixed and the boundaries of standard LCZs may be less distinct.More refined subtypes should therefore be developed on this basis to capture local thermal-environment differences.

4.4 Differentiated planning recommendations and study limitations

The two types of objective–subjective heat-exposure mismatch identified in this study represent deviations in different directions between physical heat risk and residents' subjective thermal perception.Both indicate that conventional assessment methods relying solely on temperature hotspots may overlook genuine governance needs.As shown in Figure 17, this study used the natural-breaks method and the mismatch index D to grade block-level deviations.In Low OHE–High SHE areas, Grades I and II have $D > 0$; Grade I represents the greatest deviation and is concentrated in LCZ4, LCZA, and LCZB.In High OHE–Low SHE areas, Grades III and IV have $D < 0$; Grade IV represents the most negative D value and is concentrated in LCZ1, LCZ2, LCZ3, LCZ6, and LCZ7.Grades I and IV show the most pronounced deviations and are the primary areas of concern in this study.Differentiated recommendations are proposed for these areas.

Areas I and II: Accessibility to natural cooling spaces such as parks and indoor heat-relief facilities, including medical and commercial facilities, should be prioritized.The efficiency of connections between residents' daily activity routes and these resources should be improved, and small-scale, distributed resting or shading nodes should be added in underserved areas.

Areas III and IV: These areas should not be excluded from heat-risk governance because of their relatively low SHE.High-temperature monitoring and early warning should continue based on OHE levels, while potential risk underestimation caused by long-term heat adaptation or behavioral avoidance should be considered.Objective heat exposure should retain an independent weight in the assessment system.

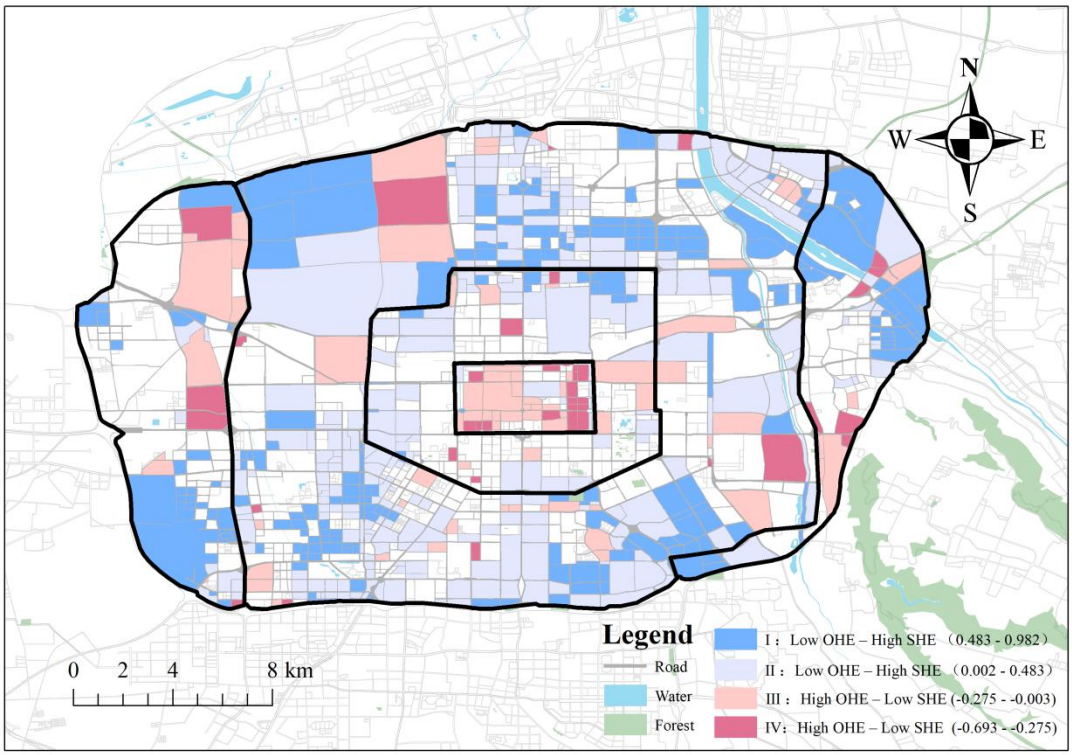


Figure 17 Graded intensity of the mismatch between objective and subjective heat exposure

This study has several limitations.First, SHE is constructed from social-media text and reflects observable public expressions of thermal perception at the urban scale rather than direct measurements of residents'

actual heat-stress experiences.It also has limited coverage of less active online groups.Therefore, SHE is more suitable for characterizing the spatial pattern of perception at the urban scale than for replacing individual-level thermal comfort surveys.The spatial mismatch between OHE and SHE should be understood as a deviation between two signals representing different dimensions, namely the "physical thermal environment" and "observable perceptual expressions," rather than as an assessment of the accuracy of OHE based on SHE.This pattern highlights spatial clues that may be overlooked by conventional temperature indicators but are actively expressed by residents, thereby providing a complementary rather than substitutive perspective for heat-risk assessment.Second, The SHE and mismatch models showed lower explanatory power than the OHE model ($R^2 \approx 0.42$ vs. 0.776), a pattern also observed across other tested models. This suggests that the selected variables capture only part of the spatial variation in SHE, and the SHAP results should therefore be interpreted as associations rather than complete explanations. Additional meteorological and behavioral factors may further improve the interpretation of SHE in future studies. Nevertheless, the identified mismatch patterns provide useful information for heat-risk management by considering both physical exposure and perceived heat risk.

5. Conclusions

Using Xi’an as a case study, this study integrated remotely sensed land surface temperature, population distribution, social-media-based thermal perception, urban morphology, and public-service data within an LCZ framework to examine the spatial mismatch between OHE and SHE. The results show that OHE and SHE are not spatially equivalent and that their mismatch exhibits clear differentiation across LCZ contexts. Compact built LCZs are predominantly characterized by High OHE–Low SHE, whereas some open and vegetated LCZs mainly exhibit Low OHE–High SHE, indicating that temperature hotspots only partially overlap with areas of stronger observable thermal perception. The associated-factor analysis further shows that OHE is primarily related to physical characteristics such as urban morphology and land cover, whereas SHE and its deviation from OHE are associated with a broader combination of physical, socioeconomic, and adaptation-related conditions. In particular, several environmental factors show different response patterns between the OHE and SHE models, suggesting that improvements in physical thermal conditions do not necessarily translate directly into corresponding reductions in perceived heat. Greater proximity to parks, healthcare facilities, and commercial services is also generally associated with smaller objective – subjective

deviations.Beyond these empirical findings, the study treats objective–subjective heat mismatch as an explicit diagnostic dimension rather than examining OHE and SHE only as parallel indicators. The LCZ framework is therefore extended from its conventional role in classifying physical thermal environments to a spatial-context framework for organizing where objective and subjective heat signals converge or diverge. This perspective complements conventional temperature-hotspot assessment by helping identify potential heat-risk blind spots that may be overlooked when urban heat governance relies primarily on physical temperature indicators. Although the specific mismatch patterns observed in Xi’an are context dependent, the proposed analytical framework provides a transferable logic for diagnosing locally specific relationships among physical heat exposure, observable thermal perception, and adaptation-related spatial conditions in other cities.

Consent to Participate declaration: not applicable

Ethics declaration: not applicable

Author contributions: Yu Zhu: Writing – review & editing, Writing – original draft, Visualization, Software, Methodology, Data curation, Formal analysis, Validation, Conceptualization. Cailan Mo: Writing – original draft, Visualization, Methodology. Zian Li: Writing – original

draft, Visualization, Methodology. Le Xuan: Software, Resources, Methodology, Conceptualization. Bingshu Zhao: Resources, Methodology, Data curation, Conceptualization. Shengyu Meng: Visualization, Investigation, Conceptualization. Hongyi Luo: Visualization, Investigation, Conceptualization. Junran Wan: Visualization, Investigation, Conceptualization. Xuhui Wang: Writing – review & editing, Validation, Supervision, Resources, Funding acquisition. Tianhui Wang: Writing – review & editing, Validation, Supervision, Resources, Funding acquisition.

Conflicts of Interest: The authors declare no conflicts of interests.

Data Availability Statement: Data are available from the corresponding author upon reasonable request.

Li, X.-X. J. S. o. t. T. E. (2020). Heat wave trends in Southeast Asia during 1979–2018: The impact of humidity. *Science of the Total Environment 721*, 137664. https://doi.org/10.1016/j.scitotenv.2020.137664

Dasgupta, P., Dayal, V., Dasgupta, R., Ebi, K. L., Heaviside, C., Joe, W., Kolli, R. K., Mehra, M. K., Mishra, A., & Raghav, P. J. T. L. P. H. (2024). Responding to heat-related health risks: the urgency of an equipoise between emergency and equity. *The Lancet Planetary Health*, *8*(11), e933-e936. http://dx.doi.org/10.1016/s2542-5196(24)00246-8

Bogdanovich, E., Guenther, L., Reichstein, M., Frank, D., Ruhrmann, G., Brenning, A., Denissen, J. M., Orth, R. J. W., Climate,, & Society. (2023). Societal attention to heat waves can indicate public health impacts. *Weather, Climate, and Society*, *15*(3), 557-569. https://doi.org/10.1175/WCAS-D-22-0147.1

Abd-Elmabod, S. K., Gui, D., Liu, Q., Liu, Y., Al-Qthanin, R. N., Jiménez-González, M. A., Jones, L. J. S. C., & Society. (2024). Seasonal environmental cooling benefits of urban green and blue spaces in arid regions. *Sustainable Cities and Society*, *115*, 105805. https://doi.org/10.1016/j.scs.2024.105805

Yin, M., He, B.-J. J. B., & Environment. (2025). Performance-based urban ventilation corridor for actual achievement of environmental benefits. *Building and Environment*, *270*, 112536. https://doi.org/10.1016/j.buildenv.2025.112536

Zhang, Q., Yang, J., Xin, J., Ren, J., Yu, W., Xiao, X., Xia, J. C. J. S. C., & Society. (2025). Cooler urban spaces? Analysis and optimization of heat-exposed landscape morphology from the perspective of local climate zones. *Sustainable Cities and Society*, 106630. https://doi.org/10.1016/j.scs.2025.106630

Sun, Z., Zhang, X., Li, Z., Liang, Y., An, X., Zhao, Y., Miao, S., Han, L., & Li, D. J. J. o. E. M. (2024). Heat exposure assessment based on high-resolution spatio-temporal data of population dynamics and temperature variations. *Journal of Environmental Management 349*, 119576. https://doi.org/10.1016/j.jenvman.2023.119576

Huang, X., Li, L., Yan, X., Ji, W., Zhao, K., & Zhao, X. J. U. C. (2024). Assessment of heat exposure risk for urban populations and spatio-temporal patterns: A perspective of urban functional zones in Xi'an, China. *Urban Climate*, *55*, 101992. https://doi.org/10.1016/j.uclim.2024.101992

Zhang, W., McManus, P., Duncan, E. J. I. j. o. e. r., & health, p. (2018). A raster-based subdividing indicator to map urban heat vulnerability: A case study in sydney, australia. *International journal of environmental research and public health*, *15*(11), 2516. https://doi.org/10.3390/ijerph15112516

Li, L., Zha, Y. J. S. C., & Society. (2020). Population exposure to extreme heat in China: Frequency, intensity, duration and temporal trends. *Sustainable Cities and Society*, *60*, 102282. https://doi.org/10.1016/j.scs.2020.102282

Hass, A. L., McCanless, K., Cooper, W., Ellis, K., Fuhrmann, C., Kintziger, K. W., Sugg, M., & Runkle, J. J. I. j. o. b. (2022). Heat exposure misclassification: Do current methods of classifying diurnal range in individually experienced temperatures and heat indices accurately reflect personal exposure? *International journal of biometeorology*, *66*(7), 1339-1348. https://doi.org/10.1007/s00484-022-02280-8

Ma, X., Lin, J., Liu, A., Nian, X., & Hong, B. J. U. C. (2024). Psychophysiological responses of the elderly to outdoor thermal stress: A focused analysis. *Urban Climate*, *57*, 102094. https://doi.org/10.1016/j.uclim.2024.102094

Zhang, T., Su, M., Hong, B., Wang, C., Li, K. J. B., & Environment. (2021). Interaction of emotional regulation and outdoor thermal perception: A pilot study in a cold region of China. *Building and Environment 198*, 107870. https://doi.org/10.1016/j.buildenv.2021.107870

Lyu, F., Zhou, L., Park, J., Baig, F., & Wang, S. J. I. J. o. G. I. S. (2024). Mapping dynamic human sentiments of heat exposure with location-based social media data. *International Journal of Geographical Information Science*, *38*(7), 1291-1314. https://doi.org/10.1080/13658816.2024.2343063

Wang, J., Meng, B., Pei, T., Du, Y., Zhang, J., Chen, S., Tian, B., & Zhi, G. J. S. o. t. T. E. (2021). Mapping the exposure and sensitivity to heat wave events in China's megacities. *Science of the Total Environment*, *755*, 142734. https://doi.org/10.1016/j.scitotenv.2020.142734

997 Liu, Q., Hang, T. J. S. C., & Society. (2025). Reassessing urban heat exposure inequity: Bridgin
998 g subjective perception and objective conditions for a more accurate understanding. *S*
999 *ustainable Cities and Society*, 106657. https://doi.org/10.1016/j.scs.2025.106657
1000 Stewart, I. D., & Oke, T. R. J. B. o. t. A. M. S. (2012). Local climate zones for urban temper
1001 ature studies. *Bulletin of the American Meteorological Society*, *93*(12), 1879-1900. http
1002 s://doi.org/10.1175/BAMS-D-11-00019.1
1003 Guo, F., Fan, G., Zhao, J., Zhang, H., Dong, J., Ma, H., Li, N. J. B., & Environment. (2025). Ur
1004 ban heat health risk inequality and its drivers based on local climate zones: A case s
1005 tudy of Qingdao, China. *Building and Environment 275*, 112827. https://doi.org/10.101
1006 6/j.buildenv.2025.112827
1007 Wang, Y., Liang, Z., Ding, J., Shen, J., Wei, F., & Li, S. J. A. (2022). Prediction of urban therm
1008 al environment based on multi-dimensional nature and urban form factors. *Atmospher*
1009 *e*, *13*(9), 1493. https://doi.org/10.3390/atmos13091493
1010 Nan, X., Zhu, H., Shu, Y., Yan, H., Middel, A., Lin, W., Ning, A., & Bao, Z. J. U. C. (2025). As
1011 sessing the impact of urban form on river-cooling dynamics: An empirical study in Ha
1012 ngzhou, China. *Urban Climate 64*, 102697. https://doi.org/10.1016/j.uclim.2025.102697
1013 Liu, Q., Hang, T., Wu, Y. J. B., & Environment. (2025). Unveiling differential impacts of multidi
1014 mensional urban morphology on heat island effect across local climate zones: Interpre
1015 table CatBoost-SHAP machine learning model. *Building and Environment*, *270*, 112574.
1016 https://doi.org/10.1016/j.buildenv.2025.112574
1017 Yang, L., Yang, C., Zhou, W., Liu, L., & Wang, C. J. J. o. C. P. (2025). Assessing heat-related h
1018 ealth risk based on the hazard–exposure–vulnerability framework in Shenzhen, China:
1019 A block-level local climate zone perspective. *Journal of Cleaner Production*, *534*, 1470
1020 36. https://doi.org/10.1016/j.jclepro.2025.147036
1021 Feng, R., Liu, S., Wang, F., Wang, K., Zhengchen, R., Wang, D. J. S. C., & Society. (2024). Fut
1022 ure urban ecological land transition and its implications for high-heat exposure in Chi
1023 na. *Sustainable Cities and Society*, *111*, 105590. https://doi.org/10.1016/j.scs.2024.1055
1024 90
1025 Subakti, A., Murfi, H., & Hariadi, N. J. J. o. b. D. (2022). The performance of BERT as data r
1026 epresentation of text clustering. *Journal of big Data*, *9*(1), 15. https://doi.org/10.1186/
1027 s40537-022-00564-9
1028 Dou, M., Wang, Y., Qiao, M., Wang, D., Gong, J., Gu, Y. J. I. J. o. A. E. O., & Geoinformation.
1029 (2024). Public responses to heatwaves in Chinese cities: A social media-based geospa
1030 tial modelling approach. *International Journal of Applied Earth Observation and Geoinf*
1031 *ormation*, *134*, 104205. https://doi.org/10.1016/j.jag.2024.104205
1032 He, P., Chen, S., Shi, G., Yu, B., Fang, H., Colaninno, N. J. B., & Environment. (2025). HP-BERT:
1033 Social Media–Based Insights into Differential Impacts of Urban Environmental Factors
1034 on Objective and Subjective Heat Exposure. *Building and Environment*, 114027. https:
1035 //doi.org/10.1016/j.buildenv.2025.114027
1036 Chen, Y., Zheng, B., & Hu, Y. J. S. (2020). Mapping local climate zones using ArcGIS-based me
1037 thod and exploring land surface temperature characteristics in Chenzhou, China. *Sustai*
1038 *nability*, *12*(7), 2974. https://doi.org/10.3390/su12072974

Yuan, B., Zhou, L., Hu, F., Zhang, Q. J. B., & Environment. (2022). Diurnal dynamics of heat exposure in Xi'an: A perspective from local climate zone. *Building and Environment*, *222*, 109400. https://doi.org/10.1016/j.buildenv.2022.109400

Zhang, Y., Zhang, J., Zhang, X., Zhou, D., & Gu, Z. J. S. (2020). Analyzing the characteristics of UHI (Urban heat island) in summer daytime based on observations on 50 sites in 11 LCZ (local climate zone) types in Xi'an, China. *Sustainability*, *13*(1), 83. https://doi.org/10.3390/su13010083

Lan, T., Liu, Y., Huang, G., Corcoran, J., Peng, J. J. S. C., & Society. (2022). Urban green space and cooling services: Opposing changes of integrated accessibility and social equity along with urbanization. *Sustainable Cities and Society*, *84*, 104005. https://doi.org/10.1016/j.scs.2022.104005

Huang, X., Hou, L., Guan, S., Li, H., Sándor, J., Albert, F., Krisztina, F. K., & Li, H. J. L. (2025). Research on the Spatio-Temporal Differentiation of Environmental Heat Exposure in the Main Urban Area of Zhengzhou Based on LCZ and the Cooling Potential of Green Infrastructure. *Land 14*(9), 1717. https://doi.org/10.3390/land14091717

Mondal, N., Anand, P. J. S. C., & Society. (2025). Influence of urbanization on heat exposure risk across Indian cities. *Sustainable Cities and Society*, 106960. https://doi.org/10.1016/j.scs.2025.106960

Zhou, R., Xu, H., Zhang, H., Zhang, J., Liu, M., He, T., Gao, J., & Li, C. J. R. S. (2022). Quantifying the relationship between 2D/3D building patterns and land surface temperature: Study on the metropolitan Shanghai. *Remote Sensing*, *14*(16), 4098. https://doi.org/10.3390/rs14164098

Liu, Q., Zhang, H., Wang, Y., Jiang, K., Shen, X., Chen, Z., Gao, Y., Shen, Y., Guo, Y. J. S. C., & Society. (2025). Unraveling nonlinear and interactive drivers of urban heat-related health risks in a mountainous coastal city. *Sustainable Cities and Society*, 107081.

Zeng, P., Sun, F., Shi, D., Liu, Y., Zhang, R., Tian, T., Che, Y. J. L., & Planning, U. (2022a). Integrating anthropogenic heat emissions and cooling accessibility to explore environmental justice in heat-related health risks in Shanghai, China. *Landscape and Urban Planning*, *226*, 104490. https://doi.org/10.1016/j.landurbplan.2022.104490

Lee, J. S., & Han, A. T. J. U. C. (2024). Heat vulnerability and spatial equity of cooling center: Planning implications from the Korean case. *Urban Climate*, *55*, 101869. https://doi.org/10.1016/j.uclim.2024.101869

He, C., Ma, L., Zhou, L., Kan, H., Zhang, Y., Ma, W., & Chen, B. J. E. i. (2019). Exploring the mechanisms of heat wave vulnerability at the urban scale based on the application of big data and artificial societies. *Environment international*, *127*, 573-583.

Prokhorenkova, L., Gusev, G., Vorobev, A., Dorogush, A. V., & Gulin, A. (2017). CatBoost: unbiased boosting with categorical features. *arXiv*. https://doi.org/10.48550/arXiv.1706.09516

Zhang, Y., Zhao, Z., & Zheng, J. J. J. o. H. (2020). CatBoost: A new approach for estimating daily reference crop evapotranspiration in arid and semi-arid regions of Northern China. *Journal of Hydrology*, *588*, 125087. https://doi.org/10.1016/j.jhydrol.2020.125087

Lundberg, S. M., & Lee, S.-I. J. A. i. n. i. p. s. (2017). A unified approach to interpreting model predictions. *Advances in neural information processing systems*, *30*. https://doi.org/10.48550/arXiv.1705.07874

Han, L., Lu, L., Fu, P., Ren, C., Cai, M., & Li, Q. J. U. C. (2023). Exploring the seasonality of surface urban heat islands using enhanced land surface temperature in a semi-arid city. *Urban Climate*, *49*, 101455. https://doi.org/10.1016/j.uclim.2023.101455

Hou, X., Xie, X., Bagan, H., Chen, C., Wang, Q., & Yoshida, T. J. R. S. (2023). Exploring spatio temporal variations in land surface temperature based on local climate zones in Shanghai from 2008 to 2020. *Remote Sensing 15*(12), 3106. https://doi.org/10.3390/rs15123106

Wang, R., Lu, T., He, B., Wang, F., Huang, Q., Qian, Z., Min, J., & Li, Y. J. S. o. T. T. E. (2024). Seasonal urban surface thermal environment analysis based on local climate zones: A case study of Chongqing. *Science of the Total Environment*, *954*, 176577. https://doi.org/10.1016/j.scitotenv.2024.176577

Xiang, Y., Tang, Y., Wang, Z., Peng, C., Huang, C., Dian, Y., Teng, M., & Zhou, Z. J. R. S. (2023). Seasonal variations of the relationship between spectral indexes and land surface temperature based on local climate zones: A study in three Yangtze River megacities. *Remote Sensing*, *15*(4), 870. https://doi.org/10.3390/rs15040870

Li, N., Yang, J., Qiao, Z., Wang, Y., & Miao, S. J. R. S. (2021). Urban thermal characteristics of local climate zones and their mitigation measures across cities in different climate zones of China. *Remote Sensing*, *13*(8), 1468. https://doi.org/10.3390/rs13081468

O'Malley, C., & Kikumoto, H. J. J. A. R. (2022). An investigation into urban heat mitigation by adopting local climate zones and land surface temperatures in the Tokyo prefecture. *Japan Architectural Review*, *5*(4), 728-739. https://doi.org/10.1002/2475-8876.12303

Kotharkar, R., Dongarsane, P. J. B., & Environment. (2024). Investigating outdoor thermal comfort variations across Local Climate Zones in Nagpur, India, using ENVI-met. *Building and Environment*, *249*, 111122. https://doi.org/10.1016/j.buildenv.2023.111122

Núñez-Peiró, M., Sanchez, C. S.-G., & González, F. J. N. J. U. C. (2021). Hourly evolution of intra-urban temperature variability across the local climate zones. The case of Madrid. *Urban Climate*, *39*, 100921. https://doi.org/10.1016/j.uclim.2021.100921

Gu, X., Beuster, L., Liu, X., van Leeuwen, E., Venverloo, T., & Duarte, F. J. N. C. (2026). Global patterns of inequality in pedestrian shade provision. *Nature Communications*. https://doi.org/10.1038/s41467-026-69190-w

Shooshtarian, S., Rajagopalan, P. J. B., & Environment. (2017). Study of thermal satisfaction in an Australian educational precinct. *Building and Environment 123*, 119-132. https://doi.org/10.1016/j.buildenv.2017.07.002

Zeng, P., Sun, F., Shi, D., Liu, Y., Zhang, R., Tian, T., Che, Y. J. L., & Planning, U. (2022b). Integrating anthropogenic heat emissions and cooling accessibility to explore environmental justice in heat-related health risks in Shanghai, China. *Landscape and Urban Planning*. https://doi.org/10.1016/j.landurbplan.2022.104490

Gasparrini, A., Guo, Y., Hashizume, M., Lavigne, E., Zanobetti, A., Schwartz, J., Tobias, A., Tong, S., Rocklöv, J., & Forsberg, B. J. T. l. (2015). Mortality risk attributable to high and low ambient temperature: a multicountry observational study. *The Lancet Planetary Health*, *386*(9991), 369-375. https://doi.org/10.1016/S0140-6736(14)62114-0

Heidenreich, A., & Thieken, A. H. J. R. a. (2024). Individual heat adaptation: Analyzing risk communication, warnings, heat risk perception, and protective behavior in three German cities. *Risk analysis*, *44*(8), 1788-1808. https://doi.org/10.1111/risa.14278

Beckmann, S. K., Hiete, M., Schneider, M., Beck, C. J. H., & Communications, S. S. (2021). Heat adaptation measures in private households: an application and adaptation of the protective action decision model. *Humanities and Social Sciences Communications*, *8*(1), 227. https://doi.org/10.1057/s41599-021-00907-6

Zhang, J., Wang, W., Rui, J., Sun, Z. J. S. C., & Society. (2026). One city, two heats: An LLM-enabled comparative analysis of heat perception, thermal environment, and health pathways in Beijing, China. *Sustainable Cities and Society*, 107330. https://doi.org/10.1016/j.scs.2026.107330

Peng, Z., Bardhan, R., Ellard, C., Steemers, K. J. B., & Environment. (2022). Urban climate walk: A stop-and-go assessment of the dynamic thermal sensation and perception in two waterfront districts in Rome, Italy. *Building and Environment*, *221*, 109267. https://doi.org/10.1016/j.buildenv.2022.109267

Schaefer, M., Salari, H. E., Köckler, H., & Thinh, N. X. J. S. o. t. t. e. (2021). Assessing local heat stress and air quality with the use of remote sensing and pedestrian perception in urban microclimate simulations. *Science of the Total Environment*, *794*, 148709. https://doi.org/10.1016/j.scitotenv.2021.148709

Li, K., Liu, X., & Bao, Y. J. F. i. E. S. (2022). Evaluating the performance of different thermal indices on quantifying outdoor thermal sensation in humid subtropical residential areas of China. *Frontiers in Environmental Science*, *10*, 1071668. https://doi.org/10.3389/fenvs.2022.1071668

Sánchez Ramos, J., Toulou, A., Guerrero Delgado, M., Palomo Amores, T. R., Castro Medina, D., & Álvarez Domínguez, S. J. A. S. (2022). Thermal resilience of citizens: comparison between thermal sensation and objective estimation in outdoor spaces: a case study in Seville, Spain. *Applied Sciences*, *12*(22), 11676. https://doi.org/10.3390/app12221167 6

Xie, Y., Wang, X., Wen, J., Geng, Y., Yan, L., Liu, S., Zhang, D., Lin, B. J. B., & Environment. (2022). Experimental study and theoretical discussion of dynamic outdoor thermal comfort in walking spaces: Effect of short-term thermal history. *Building and Environment*, *216*, 109039. https://doi.org/10.1016/j.buildenv.2022.109039

Ning, S., Jing, W., & Ge, Z. J. S. R. (2023). Sunlight perception and outdoor thermal comfort in college campuses: A new perspective. *Sci Rep*, *13*(1), 16112. https://doi.org/10.1038/s41598-023-43077-y

Wang, C., Zhang, H., Ma, Z., Yang, H., & Jia, W. J. S. (2024). Urban morphology influencing the urban heat island in the high-density city of Xi'an based on the local climate zone. *Sustainability*, *16*(10), 3946. https://doi.org/10.3390/su16103946

Song, B., Yang, L., Bai, L. J. E., & Buildings. (2025). Field experimental study of the impact of solar radiation on the thermal comfort of occupants near the glazing area in an office building. *Energy and Buildings*, *332*, 115422. https://doi.org/10.1016/j.enbuild.2025.115422

Bai, Y., Wang, M., Yan, Y., & Wang, H. (2025). Exploring the impact of 2D/3D urban morphology on land surface temperature within the diurnal cycle in Tianjin. *Sci Rep*, *15*(1), 39740. 10.1038/s41598-025-17849-7

Zhao, J., Yu, L., Zhao, L., Fu, H., Gong, P. J. S. C., & Society. (2025). Asymmetric influence of urban morphology changes on land surface temperature between daytime and nightt ime. *Sustainable Cities and Society*.

Zhang, L., Nikolopoulou, M., Guo, S., Song, D. J. B., & Environment. (2022). Impact of LCZs s patial pattern on urban heat island: A case study in Wuhan, China. *Building and Envi ronment*, *226*, 109785. https://doi.org/10.1016/j.buildenv.2022.109785

Wang, Z., Liu, Y., Wang, T., Tang, S., & Wu, X. J. U. C. (2025). Supply and demand analysis o f urban thermal environments regulation services from an accessibility perspective: A coupled thermal risk and green space cooling assessment model. *Urban Climate*, *60*, 102356. https://doi.org/10.1016/j.uclim.2025.102356

Nayak, S. G., Shrestha, S., Sheridan, S. C., Hsu, W.-H., Muscatiello, N. A., Pantea, C. I., Ross, Z., Kinney, P. L., Zdeb, M., Hwang, S.-A. A. J. J. o. t., & health. (2019). Accessibility of cooling centers to heat-vulnerable populations in New York State. *Journal of transp ort & health*, *14*, 100563. https://doi.org/10.1016/j.jth.2019.05.002

Fricke, L., & Kabisch, N. J. S. r. (2026). Impact of urban blue spaces on urban surface tempe ratures-A seasonal perspective. *Sci Rep*, *16*(1), 14697.

Hu, L., & Li, Q. J. E. R. L. (2020). Greenspace, bluespace, and their interactive influence on u rban thermal environments. *Environmental Research Letters*, *15*(3), 034041. https://doi. org/10.1088/1748-9326/ab6c30

Supplementary Files

This is a list of supplementary files associated with this preprint. Click to download.

- Supplementarymaterials.docx